Dynamic quantitative determination of intracellular sodium with fluorescence lifetime imaging

Inaugural-Dissertation

zur Erlangung des Doktorgrades

der Mathematisch-Naturwissenschaftlichen Fakultät

der Heinrich-Heine-Universität Düsseldorf

vorgelegt von

Jan Meyer

aus Hamm

Düsseldorf, Februar 2021

aus dem Institut für Neurobiologie

der Heinrich-Heine-Universität Düsseldorf

Gedruckt mit der Genehmigung der

Mathematisch-Naturwissenschaftlichen Fakultät der

Heinrich-Heine-Universität Düsseldorf

Berichterstatter:

1. Prof. Dr. rer. nat. Christine R. Rose, Heinrich-Heine-Universität Düsseldorf

2. Prof. Dr. rer. nat. Christoph Fahlke, Forschungszentrum Jülich

3. Prof. Dr. rer. nat. Jens Eilers, Universität Leipzig

Tag der mündlichen Prüfung: 09.06.2021

"When you have excluded the impossible, whatever remains, however improbable, must be the truth."

The Adventure of the Beryl Coronet / Sherlock Holmes / Sir Arthur Conan Doyle

Abstract:

Brain activity is accompanied by intracellular sodium (Na^+) transients, which have been observed under many pathological conditions including ischemic stroke or epilepsy. Recovery from these Na^+-elevations is mainly mediated by the Na^+ / K^+-ATPase (NKA) consuming energy in the form of Adenosine Triphosphate (ATP). In this study, we evaluate the relationship between global and local neuronal Na^+-signalling and ATP consumption in acute brain tissue slices of mice. Utilizing Na^+ imaging and a genetically encoded ATP nanosensor, this study was able to show that global increases in the intracellular Na^+-concentration ($[Na^+]_i$) result in transient decreases in intracellular ATP ($[ATP]_i$). In contrast, local Na^+-elevations were not accompanied by changes in $[ATP]_i$. These findings suggest, while recovery after global increases in Na^+ can temporarily surpass the cellular energy production, energy demand after local Na^+-transient can be encountered by ATP diffusion and production from unstimulated regions.

Alongside increases in $[Na^+]_i$, neuronal activity is accompanied by the efflux of K^+. The released K^+ is taken up by astrocytes and redistributed through gap junctions in the astrocytic syncytium. In this study, intensity-based fluorescent indicators and K^+-microelectrodes were used to identify a relationship between astrocyte gap junction uncoupling and the intensification of epileptic seizures. The study at hand shows, that after brief epileptiform activity K^+-uptake as well as spread via astrocytic gap junctions is reduced. We were able to identify Na^+, 2-HCO_3^-- Co-transporter (NBC) mediated alkalization as a potential cause for gap junction uncoupling and thereby identify a possible treatment against seizure intensification.

The study of these changes, was mainly performed employing fluorescent indicator dyes combined with intensity-based imaging. However, the latter can be impaired under conditions accompanied by cellular swelling (e. g. during ischemia), as changes in dye concentration interfere with proper ion quantification. To this extent, this study introduces Fluorescence lifetime imaging microscopy (FLIM) in combination with two Na^+ indicator dyes as new tools to investigate the $[Na^+]_i$, independent from the dye concetration. Employing FLIM with CoroNa Green (CoroNa) revealed significant compartmentalization of Na^+ concentrations inside human embryonic kidney (HEK) cells. However, the temporal resolution in classical FLIM (80-120 s per image) is limited by so-called dead-time artefacts, which reduce the number of usable photons. In the present study, a combination of the Na^+-indicator ION NaTRIUM Green-2 (ING-2) with a new approach, called rapidFLIM, which exhibits a drastically reduced dead-time of only ~0.5 ns was investigated. The combination of rapidFLIM with ING-2 increased the possible temporal resolution > 40 fold full frame (2 s per image) and made the first measurements of $[Na^+]_i$ under severe metabolic inhibition, which is accompanied by major cellular swelling possible. The inhibition of TRPV4 channels lead to a reduction of the Na^+ influx and nearly completely abolished cellular swelling under severe ischemic conditions.

My work showed that the combination of rapidFLIM and ING-2 is able to identify rapid changes in $[Na^+]_i$ under challenging pathophysiological conditions. Furthermore, rapidFLIM will set the stage for faster and more sensitive lifetime-based imaging with a wide variety of applications.

Zusammenfassung

Gehirnaktivität wird von intrazellulären Natriumtransienten begleitet, welche ebenfalls unter vielen pathophysiologischen Bedingungen (z.B. während Schlaganfall und Epilepsie) nachgewiesen werden konnten. Die Rückführung dieser Signale wird durch die Na^+/K^+-ATPase, unter Verbrauch von Adenosine Triphosphate (ATP) bewerkstelligt. In der vorliegenden Studie wurde der Zusammenhang zwischen globalen und lokalen Na^+-Transienten und dem Verbrauch von ATP durch die NKA untersucht. Dabei wurde Na^+-sensitive Bildgebung und ein genetisch exprimierter ATP Sensor in Gewebeschnitten des Mausgehirns verwendet. Hierbei konnte eine Reduktion der ATP-Konzentration nach globalen, jedoch nicht nach lokal begrenzten Na^+-Signale nachgewiesen werden.

Neuronale Aktivität wird auch von einem Efflux von Kaliumionen (K^+) begleitet, die wiederum von Astrozyten aufgenommen und durch so genannten Zell-Zell-Kanäle im astrozytären Synzytium verteilt werden. In dieser Studie wurde eine Beziehung zwischen dem Entkoppeln von astrozytären Zell-Zell-Kanälen und der Verstärkung epileptischer Anfälle untersucht. Hierbei konnte gezeigt werden, dass selbst nach kurzweiliger Induktion epileptischer Aktivität die astrozytenvermittelte Kaliumaufnahme, sowie Verteilung im Synzytium vermindert ist. Als möglicher Grund für das Auflösen der Zell-Zellverbindungen wurde der Na^+-Bicarbonat-Cotransporter identifiziert, welcher zu einer Alkalisierung von Astrozyten führte.

Alle bisher erwähnten Studien stützen sich auf die Kombination fluoreszierender Farbstoffe mit intensitätsbasierten Verfahren. Letztere reagieren auf Änderungen der Farbstoffkonzentration und können daher nur vermindert für die Quantifizierung von Ionen während zellulärem Schwellen (z.B. während eines Schlaganfalls) eingesetzt werden. Die vorliegende Studie erforscht die Messung von intrazellulären Na^+-Konzentrationen $[Na^+]_i$ basierend auf der Fluoreszenzlebensdauer Mikroskopie (FLIM), die unabhängig von der Farbstoffkonzentration ist. Durch die Verwendung von CoroNa Green konnte hier eine subzelluläre Kompartimentierung der $[Na^+]_i$ von menschlichen Zellen der Niere (HEK) nachgewiesen werden. Zeitlich betrachtet ist FLIM eine eher langsame Technik (80-120 s pro Bild). Die hier erbprobte Methode, rapidFLIM verbesserte mit dem Indikator ION NaTRIUM Green 2 die zeitliche Auflösung um ca. Faktor 40 (2s pro Bild). Zusätzlich ermöglichte rapidFLIM erstmals die Messung der $[Na^+]_i$ nach schwerer metabolischer Inhibition, welche von starkem zellulären Schwellen begleitet wird.

Zusammengefasst zeigt meine Arbeit, dass die Kombination aus rapidFLIM mit Na^+-sensitiven Farbstoffen rapide Veränderungen der $[Na^+]_i$ darstellen kann und das Messen auch während schwerem zellulären Schwellen ermöglicht. rapidFLIM ebnet den Weg für sensitivere, lebensdauerbasierte Messungen bei einer breiten Menge möglicher Anwendungen.

Submitted Manuscript and Publications:

Submitted Manuscript:

1. **Jan Meyer**, Niklas J. Gerkau, Karl W. Kafitz, Matthias Patting, Fabian Jolmes and Christine R. Rose (2021): rapidFLIM for dynamic lifetime-imaging with dim fluorophores at unprecedented speed. Submitted to **Nature Methods** (Impact Factor 2019/2020: 30.822) P.33-73.

Publications:

2. Mariko Onodera, **Jan Meyer**, Kota Furukawa, Yuichi Hiraoka, Tomomi Aida, Kohichi Tanaka, Kenji F. Tanaka, Christine R. Rose, and Ko Matsui (2021): Exacerbation of epilepsy by astrocyte alkalization and gap junction uncoupling. **Journal of Neuroscience** Impact factor (2021 not available), 2019: 5.673. P.74-133.

3. **Jan Meyer**, Verena Untiet, Christoph Fahlke, Thomas Gensch, and Christine R. Rose (2019): Quantitative determination of cellular [Na+]by fluorescence lifetime imaging with CoroNaGreen. **Journal of General Physiology** (Impact factor 2019: 3.628). P.134-146.

4. Niklas J. Gerkau, Rodrigo Lerchundi, Joel S. E. Nelson, Marina Lantermann, **Jan Meyer**, Johannes Hirrlinger and Christine R. Rose (2019): Relation between activity-induced intracellular sodium transients and ATP dynamics in mouse hippocampal neurons. **The Journal of Physiology** (Impact factor 2019: 4.547). P. 147-165.

Table of content:

1. Preface:

"Of all fluorescence parameters, it is the fluorescence decay function that yields the most direct insight into the molecular interactions of a fluorophore with its biological environment." - (Becker 2012)

Over the last decades, fluorescence microscopy has become a tool of utmost importance in cellular physiology. The field of application is immensely versatile, ranging from imaging of entire organisms over static immunocytochemistry in fixed tissues to dynamic 3D reconstructions beyond the diffraction limit. It became apparent that advanced microscopy techniques are needed to elucidate intracellular processes. Sodium ions (Na^+) are involved in many of these and their dynamic and quantitative measurement remains a challenging task to the present day. Monitoring the fluorescence decay function and thereby the fluorescence lifetime of Na^+-sensitive indicator dyes, is a new technique to gain insights into relevant questions in cell metabolism and physiology. "The hows and whys" of this process will be elucidated by the study in hand.

2. The cells of the brain:

The mammalian brain mainly consists of two categories of cells: neurons and glia (Fig. 1). While neurons are the more prominent (Fig. 1 A), and better-understood cell type, glial cells are much more abundant (Fig. 1 B). They amount to more than half of the cells in the mouse brain and even 90% of the human brain (Allen and Barres 2009). In comparison to glial cells, neuronal functions are clearly defined. By the conversion of chemical signals in the form of neurotransmitters to electrical signals, they are responsible for signal detection, transduction and integration (Rutecki 1992). In contrast, glial cells are historically described as passive cells, which are amongst other things accountable for the supply of energy and metabolites to neurons or the uptake of neurotransmitters. In the last decades, this knowledge has been extended by the findings that the three cell types defining this category of cells, namely astrocytes, oligodendrocytes and microglia play critical roles in synapse formation, the regulation of blood flow, axonal support as well as dynamic injury response (Barres 2008, Allen and Barres 2009, Verkhratsky and Nedergaard 2018). Neuronal and glial (especially astrocytic, also see Fig. 1 C) functions are heavily depending on each other and will be described in the following chapters.

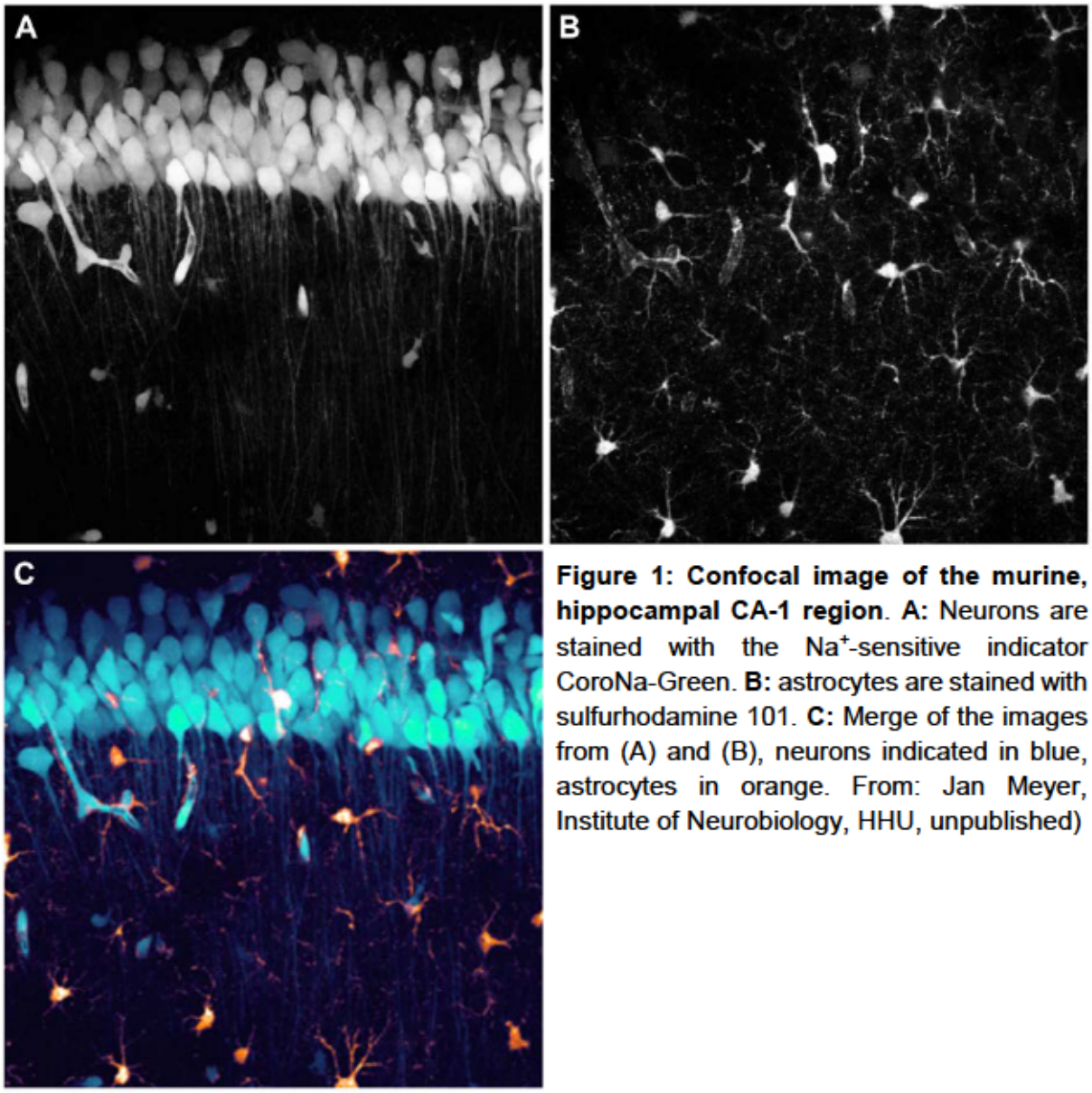

Figure 1: Confocal image of the murine, hippocampal CA-1 region. **A:** Neurons are stained with the Na^+-sensitive indicator CoroNa-Green. **B:** astrocytes are stained with sulfurhodamine 101. **C:** Merge of the images from (A) and (B), neurons indicated in blue, astrocytes in orange. From: Jan Meyer, Institute of Neurobiology, HHU, unpublished)

2.1. Neurons:

Neuronal cells are the smallest computational units of our brain (Fig. 1A). The name neuron derives from the Greek word νεῦρον (spoken neuron), meaning nerve. The term was defined by *Heinrich Wilhelm Waldecker* in 1881 and publicised by *Santiago Ramón y Cajal*. Both were prominent advocates of the neuron doctrine, which describes neurons as individual and interacting units. The followers of the rivalling, "reticular theory" believed that neurons are coupled in one large syncytium (Yuste 2015). In general, neurons consist of the soma and neurites. The latter can be subdivided in the axon and dendrites depending of the type of neurite observed. Neurons can be classified in many ways and one of them is by their anatomical polarity. Unipolar neurons only consist of the soma and one single neurite, bipolar with two neurites and multipolar with three or more neurites (Bear et al. 2008).

One subject of this study are pyramidal neurons, which are multipolar neurons and named after their pyramid shaped cell body. They occur in high numbers within the mammalian cortex and hippocampus (Bannister and Larkman 1995, Elston 2003) and consist of the soma, the basal and apical dendrite and the tuft (Fig. 2 A and B). While they receive inhibitory input at the soma and the axon, most excitatory input is mediated at dendrites from multiple origins (Cauller and Connors 1994, Spruston 2008).

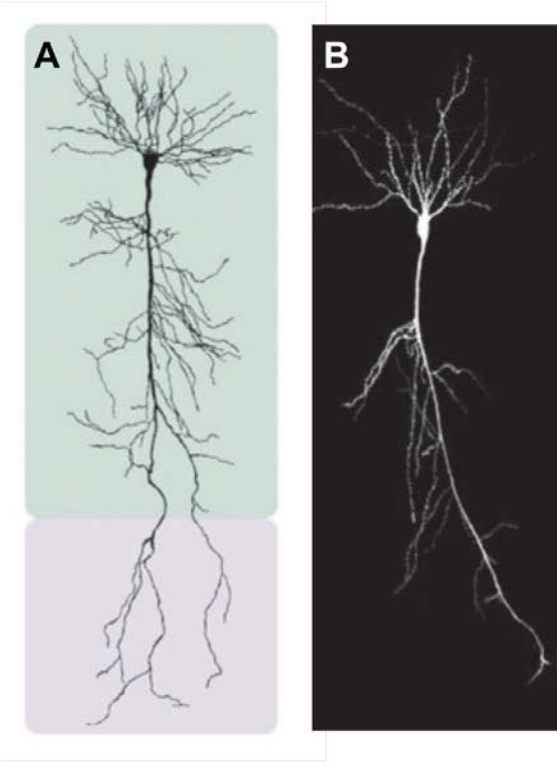

Figure 2: Hippocampal CA-1 pyramidal neurons in different levels of resolution. **A**: Schematic overview of a CA1-pyramidal neuron with the basal and apical dendrites (green) and the tuft (purple). **B** CA-1 pyramidal neuron, which was filled with SBFI via the patch-clamp technique (also see chapter 6) in an acute hippocampal tissue slice and imaged with multi photon microscopy (also see chapter 5.1).

The input, independently if inhibitory or excitatory is always mediated by synapses (also see Figure 3). Synapses are small interconnections between neurons, where the transduction from electrical to chemical signalling and back takes place (also see chapter 3.1). Synapses consist of the pre- and the postsynaptic side, both realised by protrusions of the neuronal cell membrane (Harris 1999). The latter part is also called spine and consist of the

spine head, which is connected to the dendrite by the spine neck. Spines can have a tremendous variety in size, diameter and length. Based on the length, which is realized by the spine neck morphology, spines can be sub-divided into the classes *thin*, *mushroom* and *stubby* (Nägerl et al. 2008). The implications of these variations for their physiological properties are yet to be fully understood. So far, a relationship between the morphology of the spine neck and its electrical as well as biochemical properties has been described (Tønnesen et al. 2014) .

Spines are characterized for nearly all pyramidal neurons and are almost exclusively present on dendrites (Nimchinsky et al. 2002). They are the place where neurotransmission occurs, and the tight regulation of their morphology is of absolute importance. In brief: during excitatory neurotransmission an action potential is characterized by the influx of sodium, leading to a depolarisation of the cell membrane. When this depolarisation arrives at the presynapse, voltage gated calcium channels open, resulting in the fusion of glutamate filled vesicles with the presynaptic membrane (Südhof and Rizo 2011). Thereby glutamate is released into the synaptic cleft and binds to receptors on the postsynaptic side. This again results in a Na^+-influx (in this case at the spine head) and a consequent depolarization of the postsynaptic membrane called excitatory postsynaptic potential (ePSP, Neher 2012). The released neurotransmitters need to be taken up from the synaptic cleft by specific transporters, which are driven by the inwardly directed Na^+-gradient and mainly located on perisynaptic endfeet of astrocytes (also see chapter 3.1). This process is needed to enable consecutive signal transmission and under pathophysiological conditions: counterbalance excitoxicity (e.g. in the case of stroke; Nedergaard and Dirnagl 2005).

While basic, physiological functions of neurons are gradually understood, their pathophysiological properties are still under ongoing development. In the past decades' glial cells are less and less seen as only passive counterparts and a multitude of physiologically inevitable roles were identified (Rose and Chatton 2015, Rose and Verkhratsky 2016, Verkhratsky and Nedergaard 2018).

2.2: Glia:

Glial cells were first mentioned under the term “neuroglia” by Rudolph Virchow 1827 and described as connective tissue in which the nervous system is embedded (Virchow 1970). Further, they were investigated by Camillo Golgi who described networks of “neuroglia” and also found cells connecting to blood vessels (Golgi 1870, Golgi 1885). Glial cells can be divided into multiple classes: microglia, oligodendrocytes and astrocytes (Allen and Barres 2009). Microglia play an important role in the immune competence of the brain and react to brain damage and infection (Perry and Gordon 1988). They can be *resting*, *alerted* or *reactive* depending on whether the condition of their surrounding environment is *healthy*, *lightly* or *severely damaged* respectively (Hanisch and Kettenmann 2007). Oligodendrocytes produce myelin and partly enwrap neuronal axons with it. This electrical insulation drastically improves the axonal conduction speed, resulting in heavily increased signal transmission efficiency (Salzer and Zalc 2016). Astrocytes play many important roles from signal modulation to gliotransmission and neuronal energy supply (for an extensive review see: Verkhratsky and Nedergaard 2018). A few of them will be highlighted in the following chapter.

2.2.1. Astrocytes:

The term astrocyte comes from the Greek word *astron* meaning *star* and *kyton* for *cell* and was popularized by Santiago Ramón y Cajal who invented a method to specifically stain for a glial cell specific protein around approximately 1850 (García-Marín et al. 2007). Astrocytes form a close synergy with neuronal synapses, which was termed *tripartite synapse* by Alfonso Araque (Fig. 3, Araque et al. 1999).

The specific localization of astrocytes enables the rapid uptake of neurotransmitters from the synaptic cleft and thereby shaping signal transduction. This important process is maintained by neurotransmitter transporters, present on perisynaptic endfeet of astrocytes surrounding the synapses of neighbouring neurons (Fig. 3 A and also see chapter 5, Kirischuk et al. 2016).

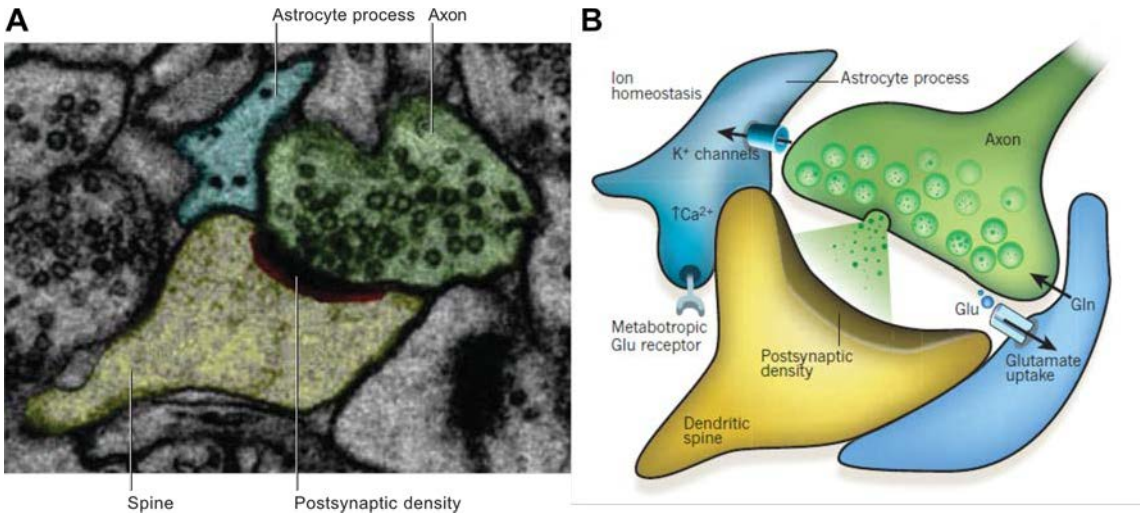

Figure 3: The tripartite Synapse. Left: Electron microscopy image of a neuronal synapse with perisynaptic, astrocytic endfeet surrounding it. The presynapse with the pool of releasable vesicles is shown in green, the postsynapse is shown in yellow with the postsynaptic density in red. The perisynaptic process of an astrocyte is shown in blue. **Right:** Scheme of the tripartite synapse in (left) using the same color scheme. Astrocytes take up glutamate (Glu) from the synaptic cleft via glutamate transporters, which is converted to the inactive glutamine (Gln) and released to the extracellular space. This Gln is than taken up by neurons and used for glutamate synthesis. Astrocytes are also involved in the regulation of the extracellular potassium concentration and react to glutamate apart from the synaptic cleft through metabotropic Glu receptors. Modified and reprinted with permission from: Eroglu and Barres (2010)

One single astrocyte can enwrap over 100.000 Synapses in the murine and around 2.000.000 synapses in the human brain (Bushong et al. 2002, Halassa et al. 2007, Oberheim et al. 2009). In the murine hippocampus which was one of the subjects of this study, astrocytes enwrap ~60% of the present synapses (Ventura and Harris 1999). At the tripartite synapse many important mechanisms are dependent on sodium. Their way of functioning will be addressed in the following chapter.

3. The sodium homeostasis:

One of the most, and if not the most fundamental principle of our brain is the heterogeneous distribution of ions across the cellular membrane. The resulting electrochemical gradients between the intra- and extracellular space fuel a plethora of processes. Most cells, with only a few exceptions, have a very similar cation composition in the intracellular space. The intracellular K^+-concentration ($[K^+]_i$) is high, the Na^+-concentration ($[Na^+]_i$) is around ten times

lower and Ca^{2+} is present in a low nanomolar concentration (for astrocytes see Fig. 1, Rose and Verkhratsky 2016).

This distinct feature very likely developed due to the ionic composition of the primeval oceans and is existent till the present day (Kazmierczak et al. 2013). The driving force for each ion can be calculated by the Nernst equation:

$$E_x = \frac{RT}{ZF} ln \frac{[X]_0}{[X]_i}$$

R is the gas constant, F the absolute temperature, Z the ion's valence, F the Faraday's constant, $[X]_0$ is the ion concentration for the extracellular and $[X]_i$ for the intracellular space. It calculates the equilibrium potential (E_X) at which the electrostatic forces are equal to the concentration gradient forces (Rutecki 1992). The equilibrium potentials for e.g., Na^+ and Ca^{2+} are positive, meaning that the cations will flow into the cell once a permeable pathway (e.g. a channel) is opened.

Sodium has a high extracellular concentration of around 150 mM and a low intracellular concentration of ~ 12 -15 mM in neurons and astrocytes (see Fig. 4) (Rose and Chatton 2015, Mondragao et al. 2016, Ziemens et al. 2019). The ubiquitously expressed Na^+, K^+ ATPase (NKA) maintains this steep inwardly directed, electrochemical gradient. Here, one ATP is hydrolysed to ADP and free phosphate, while the export of 3 Na^+ and the import of 2 K^+ takes place (Skou and Esmann 1992). As many processes are coupled to the inwardly directed sodium gradient, the NKA is constantly re-establishes this gradient. It has been shown, that an inhibition of the NKA with specific antagonists (e.g. Ouabain) or the removal of extracellular K^+ immediately leads to an increase in $[Na^+]_i$ (Walz and Hertz 1984, Rose and Ransom 1996).

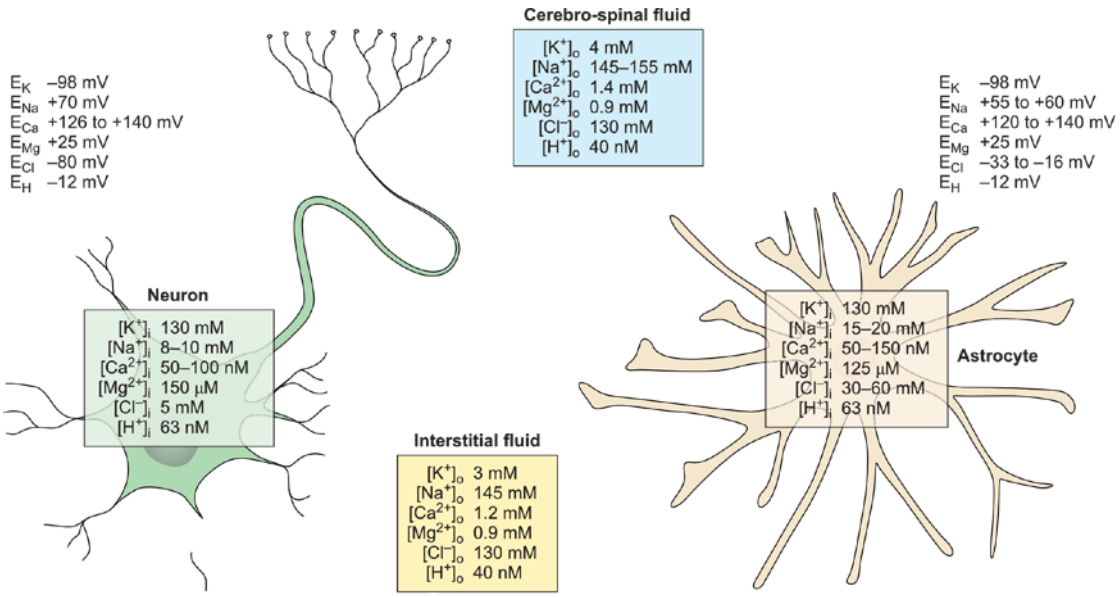

Figure 4: The ion composition of the extra- and intracellular space. Schematic drawing of a neuron and an astrocyte and their respective intracellular ion concentrations. Using the Nernst-equation and the extracellular concentrations, the driving force for each ion (Nernst-potential) can be calculated. When its positive, the respective ion will flow into of the cell and the other way round when negative. Additionally, the extracellular concentrations for the cerebro-spinal and interstitial fluid is depicted. Reprinted with permission from: (Verkhratsky and Nedergaard 2018)

Na^+ also plays an important role in signal transmission and transduction. Former studies pointed out, that neuronal signals are also accompanied by intracellular elevations of Na^+ in astrocytes (Rose and Ransom 1996, Rose et al. 1998). Neuron-glia interaction is in many cases sodium mediated. To this extent the following chapter will highlight the significance of sodium for many intracellular processes.

3.1 The importance of sodium in intracellular processes:

The regulation of ion gradients across the membrane is in most cases coupled to sodium. As many of the involved transport processes can operate in both directions (called forward- and reverse mode) the $[Na^+]_i$ is often the determining factor if the co-transported ions are imported or exported. In contrast to Na^+, K^+ has a high intracellular and low extracellular concentration and is as well mediated by the NKA. Membrane flux can e.g. occur via Kir 4.1 channels or the Na^+, K^+, $2Cl^-$ Cotransporter (NKCC1, see Fig. 5). The latter is, to an even larger extent, also important for the Cl^- homeostasis and imports 1 Na^+, 1 K^+ and 2 Cl^- (Ben-Ari 2014).

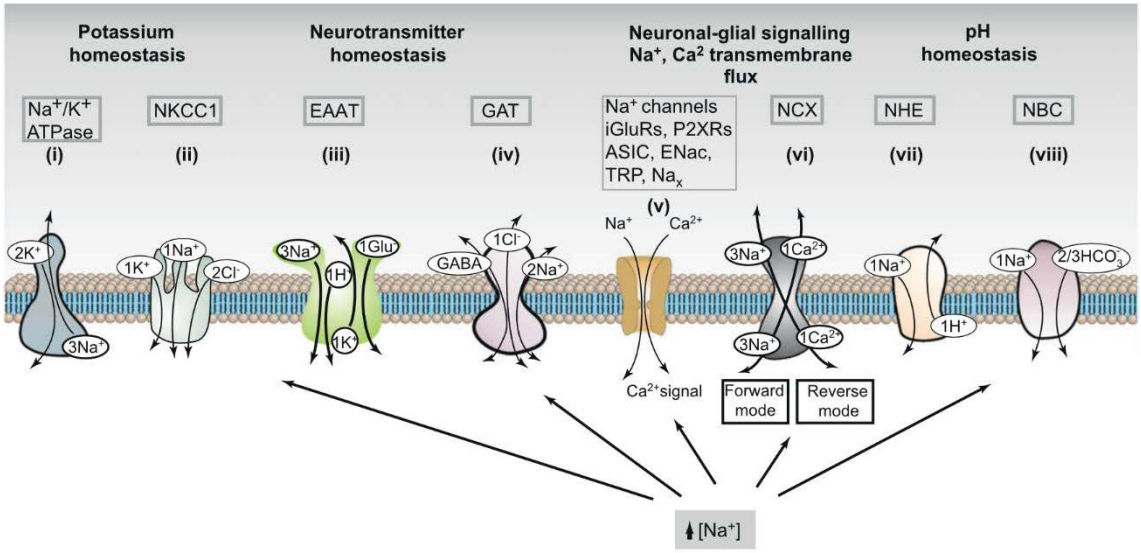

Figure 5: Pathways that are coupled to the $[Na^+]_i$. Chloride and Potassium are imported together with sodium by the Sodium, Potassium, 2 Chloride Cotransporter (NKCC1). Neurotransmitter clearance is amongst others mediated by the excitatory amino acid transporter (EAAT) or GABA transporters for excitatory or inhibitory neurotransmission respectively. Neuron-Glia interaction can occur through a multitude of sodium permeable channels e.g. ionotropic glutamate receptors (iGluRs) and also calcium homeostasis is coupled to sodium by the Na^+- Ca^{2+}-Exchanger (NCX). pH is also controlled sodium dependently, as the Na^+-, H^+-exchanger and the sodium bi-carbonate exchanger are both coupled to the inwardly directed sodium gradient. All the aforementioned pathways increase the $[Na^+]_i$. The excess Na^+ needs to be pumped out of the cell again, which is exclusively maintained by the Na^+, K^+-ATPase. Modified and reprinted with permission from: (Kirischuk et al. 2012).

The NKCC1 plays an important role in the maturation of neurons as its expression profile varies with age (Rivera et al. 1999). Before P14, NKCC1 is more broadly expressed than the chloride exporting cotransporter KCC2 (K^+, Cl^- Cotransporter). After P14 the relation between NKCC1 and KCC2 switches, leading to a reduction in intracellular Cl^- (Ben-Ari et al. 2012). The high $[Cl^-]_i$ in the juvenile brain results in an excitatory effect of GABA during early network formation (Kettenmann et al. 1984, Meier et al. 2008, Untiet et al. 2017).

Na^+-ions play a critical role in signal transmission. It has been shown that action potential generation and propagation is mediated by Na^+ in plentiful types of neuronal axons (Jaffe et al. 1992, Rose and Konnerth 2001). For excitatory neurotransmission, glutamate is the most abundant neurotransmitter in the nervous system. The depolarization of the presynaptic membrane results in the release of glutamate into the synaptic left (also see chapter 2.1). Here it binds to the ionotropic glutamate receptors NMDA, AMPA and kainate (Fig. 6) which all are permeable for Na^+. The first receptors which open to this binding, are AMPA and kainate receptors. Both have fast channel opening times but low channel conductivity, resulting in a small depolarization of the postsynaptic membrane. Under resting membrane potential (-40 to

-70 mV) NMDA receptors are blocked by Mg^{2} (Verkhratsky and Kirchhoff 2007). The depolarization induced by AMPA and kainate receptor activation, removes this blockage and thereby opens the slower but larger influx component (Spruston et al. 1995). Na^+-influx is the main charge carrier in all three cases, rendering the electrochemical Na^+-gradient of utmost importance for signal transduction and transmission.

To counteract over-excitation and enable subsequent signal transmission, the released glutamate needs to be taken up rapidly (Fig. 6). This uptake is accomplished by the family of excitatory amino acid transporters (EAAT) of which 5 versions (EAAT1-5) have been found (Danbolt 2001).

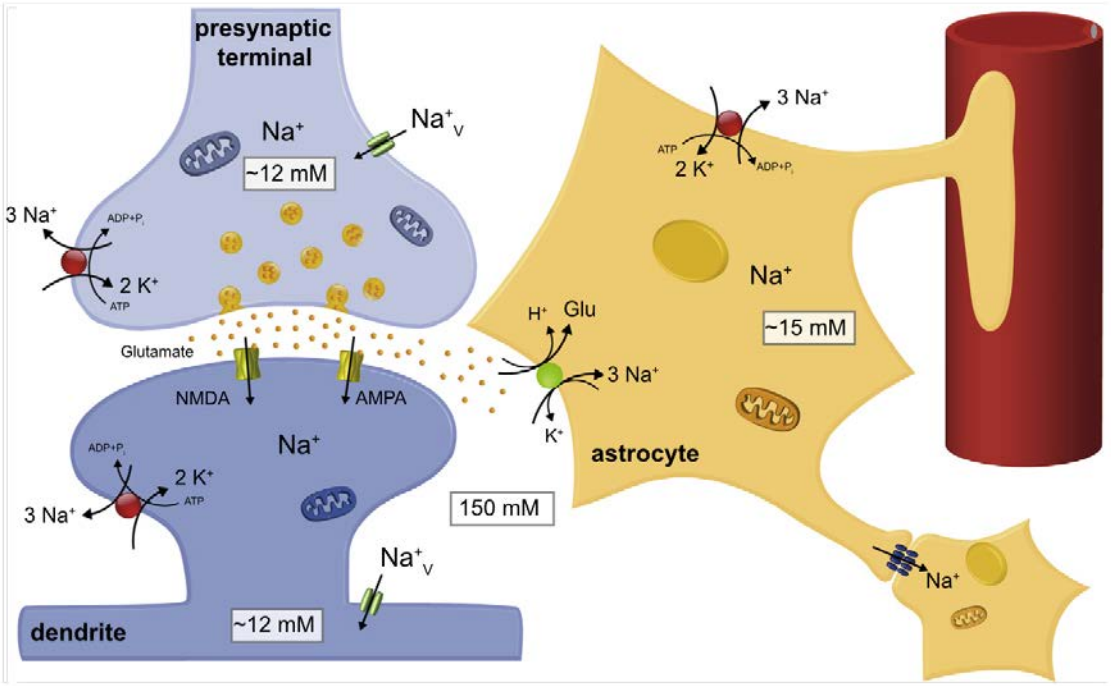

Figure 6: Sodium dynamics at the tripartite synapse. Upon depolarization of the presynaptic terminal via voltage-gated Na^+-channels (Na_V), Ca^{2+} enters the cell (through voltage-dependent Ca^{2+}-Channels, Ca_V, not shown), resulting in the fusion of glutamate filled vesicles with the presynaptic membrane. Thereby, glutamate is released into the synaptic cleft and can consecutively activate ionotropic glutamate receptors (NMDA and AMPA). Consequently, Na^+ enters the postsynapse, resulting in an excitatory postsynaptic potential (ePSP). The glutamate needs to be cleared from the synaptic cleft to A) encounter overexcitation and B) enable consecutive synaptic transmission. This is mainly done by glutamate transporters present on perisynaptic, astrocytic endfeet. All the aforementioned processes increase the intracellular $[Na^+]i$ and thereby reduce the sodium gradient between the intra- and extra-cellular space. The latter then needs to be restored by the ubiquitously expressed Na^+- K^+-ATPase (NKA). Reprinted with permission from Rose and Chatton 2016.

Astrocytic EAAT1 and 2 (mouse analogue: Glutamate aspartate transporter, GLAST and Glutamate transporter-1, GLT-1) accomplish approximately 90% of this uptake (Danbolt 2001, Karus et al. 2017). The influx of 3 Na^+, 1 H^+ and the efflux of 1 potassium drives the transport of 1 Glutamate from the extra- to the intracellular space (Zerangue and Kavanaugh 1996). The uptake process is highly dependent on the $[Na^+]_i$ as an increase of 20 mM Na^+ reduces the driving force for glutamate already by ~ 13 fold (Unichenko et al. 2012, Kirischuk et al. 2016). The inwardly transported glutamate can either be amidated by the glutamine synthetase to glutamine (Martinez-Hernandez et al. 1977) or deaminated to α-ketoglutarate and enter the Tri-carboxylic-acid cycle (McKenna 2007). The non-reactive glutamine is released into the extracellular space and consecutively taken up by neurons.

The process of Glutamate uptake in astrocytes, conversion to and release of glutamine with the re-uptake and re-conversion to glutamate in neurons is called Glutamate-glutamine cycle (Hertz et al. 1999, Bröer and Brookes 2001, Chaudhry et al. 2002). The $[Na^+]_i$ directly controls the release of glutamine and could thereby modulate the levels of excitatory synaptic transmission (Billups et al. 2013, Kirischuk et al. 2016). Another important ion, when talking about neuronal communication, is Ca^{2+}. The influx of Ca^{2+} into the presynapse triggers the so called SNARE-complex at the presynaptic terminal, resulting in the fusion of neurotransmitter filled vesicles. The Ca^+-homeostasis is connected to Na^+ by the Na^+-, Ca^{2+}-Exchanger (NCX, see Figure 4), importing 3 Na^+ while exporting 1 Ca^{2+} (Blaustein and Lederer 1999). The reversal potential of the NCX is very close to the membrane potential of neurons and astrocytes. Therefore it can easily change its transport direction and thereby act as a Na^+-extruding mechanism with a potentially neuroprotective influence on pathophysiological conditions (Paluzzi et al. 2007, Rojas et al. 2007, Gerkau et al. 2017).

In addition to the aforementioned processes, pH is regulated by Na^+-dependent transport mechanisms. This is maintained by the Na^+, H^+-exchanger (NHE, see Fig. 5), that has a stoichiometry of 1 H^+ to 1 Na^+ and the Na^+-, HCO_3^-- cotransporter (NBC), which can transport 1 Na^+ together with 2 or 3 HCO_3^- (Deitmer and Rose 1996). Whereas the NBC can work in forward and reverse mode (Theparambil et al. 2015), under physiological circumstances the NHE only works in forward mode (Fig. 5). As a result the NBC either imports or exports HCO_3^- depending on the $[Na^+]_i$ (also see chapter 5), the NHE only expels H^+ from the intracellular space (Orlowski and Grinstein 1997).

All of the here described mechanisms are dependent on the $[Na^+]_i$ and thereby highlight the importance of understanding sodium dynamics in cells. They increase the $[Na^+]_i$ and thereby reduce the electrochemical Na^+ gradient. The exact measurement of the resting $[Na^+]_i$ or changes in it, is therefore vital to investigate physiological and pathophysiological conditions.

In recent decades many Na^+-dependent mechanisms in different cellular preparations have been investigated (e.g., Rose and Ransom 1996, Fleidervish et al. 2010, Langer et al. 2012, Gerkau et al. 2018, Ziemens et al. 2019). However, Na^+-signalling is far from being fully understood. The present study will elucidate critical aspects in the relationship between Na^+-signalling and ATP consumption in neurons, evaluate Na^+-signalling in astrocytes and thereby investigate a cause for astrocyte gap junction uncoupling as well as propose a new method for Na^+-quantification, independent of the dye concentration. The last-mentioned will pave the way for a broader understanding of intracellular Na^+-dynamics utilizing Fluorescence Lifetime Imaging Microscopy (FLIM).

4. Imaging intracellular sodium in the living brain

In this study, indicators that change their properties upon binding to their respective ion (or metabolite) were used to investigate changes in ion and metabolite concentration of the intracellular space during resting and active conditions. For many ions and some metabolites (e.g. Ca^+, K^+, pH, ATP and pyruvate) indicators are available that can be encoded genetically (Rochefort and Konnerth 2008, Lin and Schnitzer 2016, Bischof et al. 2017, Lerchundi et al. 2019). In comparison to that, no genetically encoded Na^+-sensors are described and chemical, Na^+-sensitive indicator dyes need to be used instead. In the following chapters, sodium indicators will be used to investigate Na^+-signalling in various cell types.

One of the most frequently used sodium indicators is sodium-binding benzofuran isophthalate (SBFI, Minta and Tsien 1989). A major difficulty concerning sodium-based imaging is the high resting $[Na^+]_i$ (approx. 8-15 mM in neurons and astrocytes, also see chapter 3) compared to calcium-based imaging, where resting calcium is in the low nanomolar range. Up to now, SBFI has been utilized in many studies, ranging from widefield applications in cell culture (Rose and Ransom 1996, Rose and Ransom 1997) and acute brain tissue slices (Callaway and Ross 1997, Langer and Rose 2009, Mondragao et al. 2016, Gerkau et al. 2018, Ziemens et al. 2019), to laser scanning microscopy in dendrites and spines (Rose et al. 1999, Rose and Konnerth 2001, Rose 2002, Gerkau et al. 2019). SBFI can be imaged at ~340 nm, where it exhibits nearly no sodium sensitivity (isosbestic point), and at ~380 nm were it has a high sodium sensitivity. Dividing the insensitive by the sensitive wavelength, results in a ratio that is sensitive to sodium but impervious for secondary factors like bleaching or to some extent changes in focus. So called ratiometric imaging is nearly exclusively used in widefield configuration, where optical resolution is limited. High resolution imaging with SBFI requires

either specialized UV-lasers in the below 400 nm range or expensive and high-maintenance multiphoton lasers.

Multiphoton excitation utilizes the fact that a fluorophore can absorb two photons of a longer wavelength (typically two times longer the excitation maximum) within a time-window of 0.5 fs and hence reach the excited state (Lakowicz 2006).This is realized by highly pulsed lasers (> 80 MHz) and with short pulse widths (<100 fs, Denk et al. 1990, Helmchen and Denk 2005).

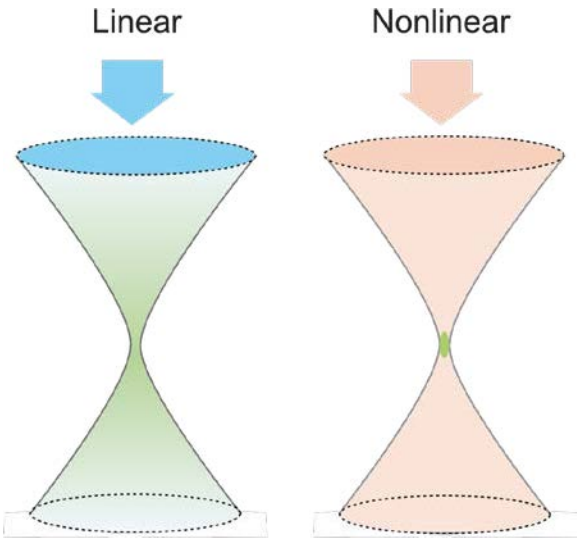

Figure 7: The underlying principles of multiphoton excitation. The difference between linear (single-photon excitation) and nonlinear excitation (multi-photon excitation) is the size of the excited volume. While in linear excitation, the excited volume is large and affecting the whole light pathway; in nonlinear excitation only the focal plane will have a high enough photon density to excite fluorophores. Reprinted with permission from: (Helmchen and Denk 2005)

The resulting excitation is locally confined in the focal plane, where the photon density is high enough to reach the nearly simultaneous absorption of two photons (see Fig. 7, Helmchen and Denk 2005). The benefit of this complex task is a drastically improved spatial resolution, due to reduced scattering in the above and below tissue, while simultaneously reducing photodamage (Denk and Svoboda 1997). Multi-photon excitation has been used in a broad field of applications where high spatial resolution or deep tissue penetration is a necessity, e.g. in fine dendrites and spines of neurons or for *in vivo* imaging (Denk et al. 1995, Denk et al. 1996, Rose et al. 1999, Svoboda et al. 1999, Yuste et al. 1999, Rose and Konnerth 2001, Gerkau et al. 2018).

5. Activity induced sodium signalling in neurons:

In the study at hand, we utilized above mentioned intensity-based imaging with SBFI and FRET imaging (for detailed methods see: Imamura et al. 2009, Algar et al. 2019) with the genetically encoded nanosensor ATeam1.03YEMK to elucidate the relationship between different patterns of intracellular Na^+-signals and ATP in CA-1 pyramidal neurons.

Excitatory neurotransmission increases the $[Na^+]_i$, which reduces the sodium gradient and thereby the driving force for a plethora of processes. The re-establishment of this gradient is maintained by the NKA. Here, we apply a model for recurrent network activity, were the Mg^{2+}-block of NMDA receptors is removed and GABAergic inhibition is reduced (0 Mg2+ / BIC-Model, see Karus et al. 2015). Using this model, results in repetitive, global neuronal Na^+-signals (Fig. 8A). The resulting NKA activity is exceeding intracellular ATP ($[ATP_i]$) production capabilities, leading to a slow but a steady reduction in $[ATP]_i$ (Fig. 8B, Gerkau et al. 2019).

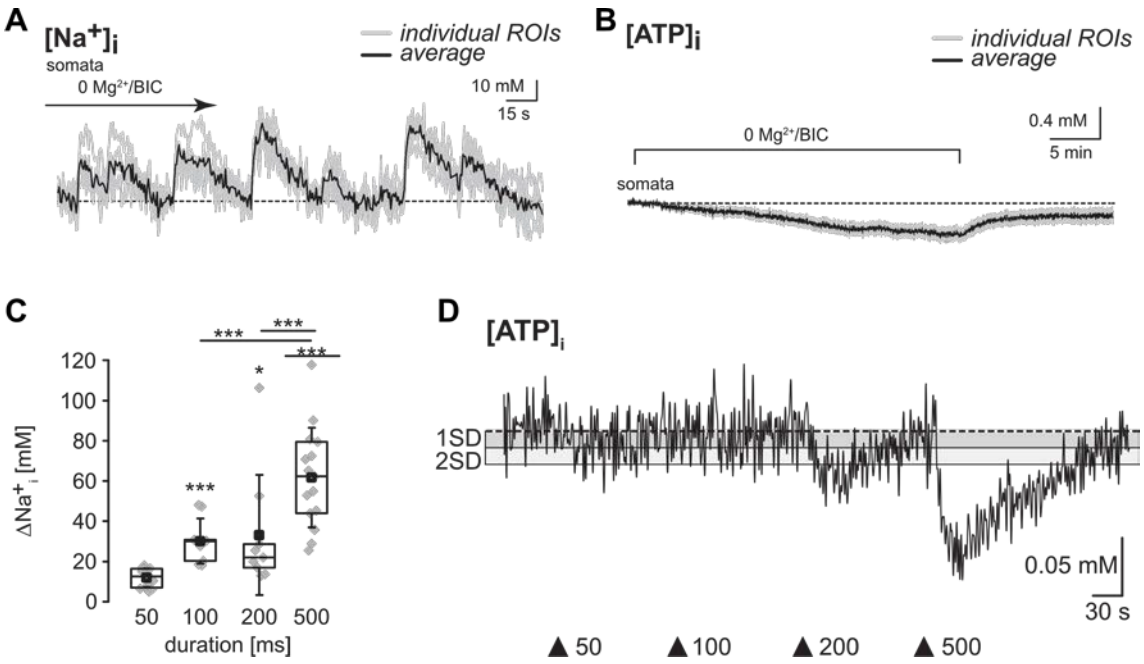

Figure 8: Changes in intracellular Na^+ and ATP during different patterns of neuronal signalling. A: Application of a model for recurrent network activity, where the Mg^{2+}-blockage of NMDA receptors is removed and GABA-receptors are inhibited, resulting in repetitive elevations in $[Na^+]_i$. **B:** Same experiment as in (A), but the $[ATP]_i$ is depicted. Using the recurrent network model resulted in a slow, steady and transient decrease in $[ATP]_i$ **C:** Box-and-whisker plots showing increases in intracellular Na^+ upon focal application of glutamate (in 10 µm distance to the dendrite) at 50, 100, 200 and 500 ms application duration. Mean: black square, median: black line, box: interquartile range whiskers: standard deviation, individual data point in grey. Note the distinct increase in sodium amplitude with increasing application duration. **D**: Same experiment as in (C) but measuring the intracellular ATP concentration. Note that only extensive, and not confined application of more than 200 ms resulted in resolvable ATP transients. Modified and reprinted with permission from Gerkau et al. (2019).

The same was the case after global increases in $[Na^+]_i$ (e.g. induced by global application of glutamate). The ATP consumption during NKA activity can temporarily exceed ATP production, resulting in a drop of intracellular ATP levels (Gerkau et al. 2019). However, local increases in Na^+ (e.g. induced by focal application of glutamate, Fig. 8C) did not alter the ATP concentration, suggesting that local ATP consumption can be encountered with ATP production and diffusion from unstimulated parts of the cell (Fig. 8D, Gerkau et al. 2019).

In summary, the results of the present study show that global Na^+-signalling in neurons results in a drop in cellular ATP, whereas during locally confined sodium signalling, the ATP consumption of the NKA does not exceed intracellular ATP production capabilities (Gerkau et al. 2019).

6. Activity induced sodium signalling in astrocytes

Neuronal sodium signalling is also accompanied by increases in extracellular K^+ ($[K^+]_e$). After depolarization, voltage-gated K^+-channels open and K^+ flows out of the cells, leading to the repolarization of the neuronal membrane (Bear et al. 2008). One important function of astrocytes is the uptake of K^+, present in the extracellular space after the firing of neuronal action potentials (also see Fig 3B and 6). Under pathophysiological conditions, this extracellular K^+ can accumulate, resulting in hyperexcitability of neurons and leading to even more increased levels in $[K^+]_e$. Astrocytes form a large syncytium with neighbouring astrocytes over specialized channels called *gap junctions.* After the extracellular K^+ is taken up, it is redistributed from regions with high concentrations to regions with low concentrations, a process called *spatial buffering* (Hirase et al. 2004, Wallraff et al. 2006, Langer et al. 2012). Hyperexcitability plays a big role in epilepsy, a disease that is characterized by seizures, leading to excessive firing of action potentials in neurons. Gap junction uncoupling in astrocytes and thereby reduced K^+-clearance might be one reason for the increased hyperactivity (Bellot-Saez et al. 2017). In the present study, we address the question together with colleagues and propose a potential mechanism for astrocyte uncoupling.

Using ion sensitive microelectrodes (for detailed description see: Haack et al. 2015) and intensity based imaging, we were able to measure a potential reduction in K^+-clearance after short periods of induced epileptiform activity (Onodera et al. 2021). This hypothesis could be reinforced, as a we were able to verify an uncoupling of astrocytes after epileptiform discharges by measuring a reduced diffusion of Na^+ through the astrocytic network (Fig. 9, Onodera et al. 2021).

Additionally, this study shows, that even these brief episodes of induced epileptiform activity lead to Na^+/HCO_3^- co-transporter (NBC) activation and thereby intracellular alkalization of astrocytes. The latter, resulting in partial gap junction uncoupling (Onodera et al. 2021).

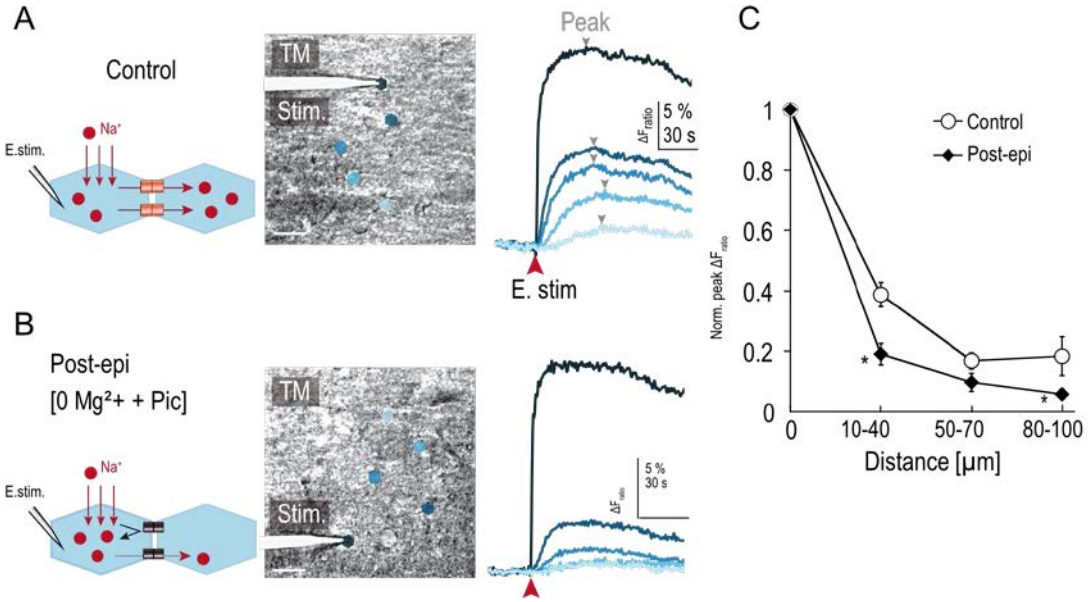

Figure. 9: Reduction in astrocytic gap junction coupling after brief epileptiform activity A: Electrical stimulation results in an increase in intracellular sodium (here measured with SBFI intensity), not only in the stimulated but also neighbouring astrocytes. **B:** Same experiment as in (A), after the perfusion with a model for recurrent network activity (0Mg2+ / PIC). After brief epileptiform activity, the spread of sodium was drastically reduced. **C:** The normalized peak fluorescence intensity is plotted against the distance of neighbouring astrocytes revealing a significant reduction in Na^+-spread after short periods of recurrent network activity, which indicates a reduction in astrocyte gap junction coupling. Modified and reprinted with permission from (Onodera et al. 2021).

The results presented in this study show, that blocking the NBC resulted in a dampening of intracellular alkalization of astrocytes and thereby preventing astrocyte uncoupling and hyperactivity intensification, both in vitro and in vivo (Onodera et al. 2021).

The NBC addressed here, is a sodium dependent transporter, which imports or exports 1 Na^+ together with 2 or 3 HCO_3^- (also see chapter 3.1; Deitmer and Rose 1996). Depending on the $[Na^+]_i$, the NBC can work in forward and reverse mode (Theparambil et al. 2015). Resulting from that, the $[Na^+]_i$ plays an important role in the regulation of intracellular pH. The exact measurement of the resting $[Na^+]_i$ or changes in it, is therefore vital to investigate physiological and pathophysiological conditions. All the aforementioned studies utilize intensity based imaging to quantify changes in the $[Na^+]_i$, which can be prone to secondary factors that can occur when observing living tissue under pathophysiological conditions, like changes in focus, cell volume or bleaching.

One way to break through these obstacles, is utilizing the fluorescence lifetime instead of the intensity. In the study at hand, we combine Fluorescence lifetime imaging microscopy (FLIM) with Na^+-sensitive indicator dyes, and investigate resting cellular Na^+ levels as well as rapid changes in it.

7. Fluorescence lifetime imaging microscopy:

The term fluorescence goes back to 1852 when Sir George Gabriel Stokes first described the phenomenon that a fluorophore excited with a specific wavelength (e.g. in the case of ING-2, 488 nm) will emit light *shifted* to a longer wavelength (e.g. in the case of ING-2, ~540 nm). This, process termed *stokes shift* (Stokes 1852), is best described by a *Jablonski Diagram* (See Fig. 10, Lichtman and Conchello 2005, Lakowicz 2006).

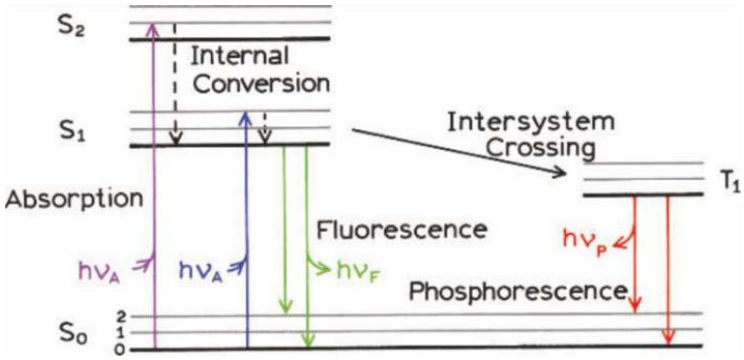

Figure 10: Jablonski Diagram. Possible photon pathways of a fluorophore between the absorption and the emission of a photon. Before excitation the fluorophore is in the ground state (S_0), after excitation it enters an energetically higher state (S_1 or S_2) and either emits photons (fluorescence) or undergoes internal conversion to re-enter S_0. Reprinted with permission from (Lakowicz 2006)

A fluorophore can have three different singlet states, which correspond to different states of vibrational energy. S_0 is the ground state, S_1 the first and S_2 the second electronic state. Following the absorption ($h\nu_{A)}$ of light, the fluorophore is excited to a higher vibrational level and therefore singlet state. From the S1 or S2 state, the energy can relax in multiple ways (Fig. 8). The most prominent is the emission of photons (fluorescence, $h\nu_F$), while relaxing the fluorophore back to the ground state. In the second route, the fluorophore enters a triplet state and emits photons at a much longer wavelength (called phosphorescence, Jablonski 1933, Jabłoński 1935). The duration needed for the individual routes can differ vastly. While internal conversion or vibrational relaxation does only take a few picoseconds (ps), the emission of fluorescence is typically in the pico- to nanosecond (ps to ns) and phosphorescence even in the microsecond (µs) range (Lichtman and Conchello 2005). The time that the fluorophore

stays in the excited stated state is called fluorescence lifetime (τ), whereas the amount of photons emitted is the fluorescence intensity (I, Lakowicz 2006). Resulting from the different routes of relaxation, the specific lifetime is a statistically distributed effect based on the way the energy was converted. The technique used in this study is based on time domain measurements and counts each incoming photon in a time correlated manner, hence the name Time Correlated Single Photon Counting (TCSPC, see Fig. 11)

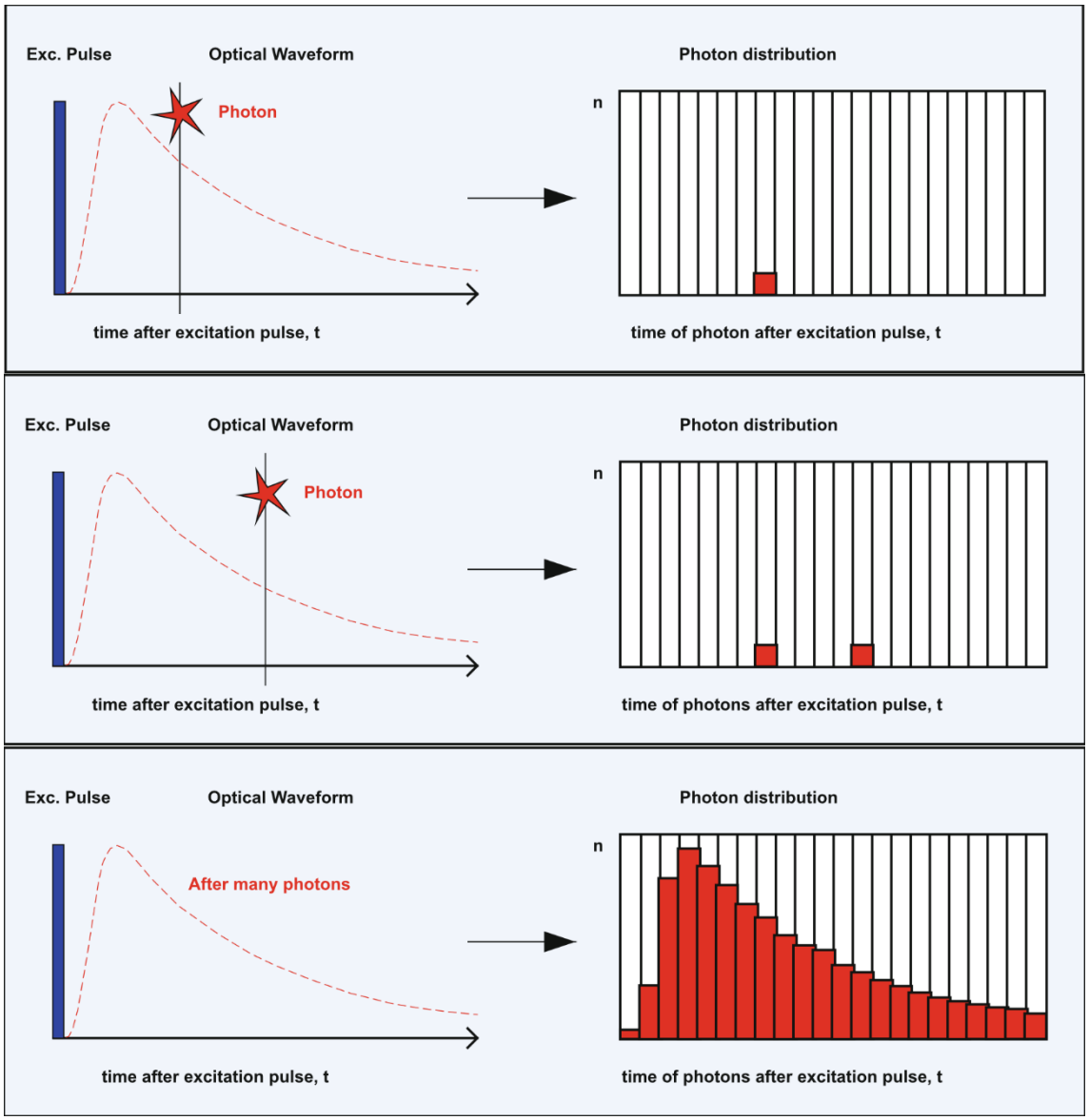

Figure 11: Principle of Time Correlated Single Photon Counting (TCSPC) Top: Simplified detector signal after one excitation pulse. Excitation is shown in blue, emission is shown in red. Note the short excitation pulse needed in the low ps range. **Middle:** Detector after the second excitation. Due to the statistical nature of the emission process incoming photons have different lifetimes. Multiple Photons (usually >1000) are needed to obtain enough information about the explicit lifetime (τ) **Bottom:** Example of a photon distribution specific for a certain dye. By fitting a exponential decay to this distribution, the specific τ can be calculated. Reprinted with permission from (Becker 2015)

In TCSPC the time between the excitation pulse and the arrival times of the probes emitted photons are registered and saved in a time-correlated manner (Becker 2015). Because of the aforementioned routes of relaxation, the lifetime of an individual photon varies, when collecting the same sample over a certain time. When counting enough photons (typical >1000 photons), a distribution unique to the observed fluorophore can be obtained (see Fig. 9). This photon distribution can then be analysed in many different ways. One of them is by iterative reconvolution of the IRF with a multi-exponential model function (Becker 2015). TCSPC is based on the principle that the arrival time of the photon in relation to the time point of the excitation pulse is equal to its lifetime. As the arrival times of all incoming photons are always seen relatively to their excitation pulse, an excitation source with a high pulse repetition rate (>20 MHz) is a necessity. The most sophisticated way uses femtosecond, high repetition (>80 MHz) multiphoton lasers and combine high resolution imaging with optimal timing and high photon throughput.

In intensity-based imaging, the observed value (I) is in most cases directly dependent on the number of photons and thereby indirectly on the concentration of the observed fluorophore. In FLIM, increasing or decreasing the number of photons (or indirectly the concentration of fluorophore) affects the goodness of the fit and thereby only results in changes in the signal to noise ratio (Liu et al. 2019). Resulting from that, τ is robust against possible changes in dye concentration and other secondary factors that e.g. can occur during physiological imaging.

8. Combination of FLIM and Na^+ sensitive indicators

As stated before, sodium is crucial for a multitude of intracellular processes (see chapter 3). The $[Na^+]_i$ sets the driving direction for many transport-processes and is therefore of immense importance (Rose and Karus 2013, Rose and Chatton 2015). The $[Na^+]_i$ in neurons and astrocytes has been estimated at ~8-15 mM (Mondragao et al. 2016, Ziemens et al. 2019), but up to now this has only been done for single cell studies and only somatic Na^+ was quantified. The driving direction of neurotransmitter transporters is especially important when observing fine perisynaptic processes of astrocytes or neuronal dendrites and spines. Here, a reversal of these transporters would directly affect signal transmission. Another important transporter coupled to the Na^+-gradient is the NCX. It was shown that even brief, local applications of NMDA can result in NCX reversal, contributing to local Ca^{2+}-signalling (Ziemens et al. 2019).

The quantification of $[Na^+]_i$ is challenging and often relies on intensity-based imaging, where only changes in $[Na^+]_i$ can be reliably determined (also see chapter 5, Rose and Konnerth

2001, Rose 2002, Ona-Jodar et al. 2017, Gerkau et al. 2019). FLIM in combination with Na^+-sensitive indicators might be a promising technique to elucidate the $[Na^+]_i$ under these challenging conditions. To this extent, I extensively studied the suitability of CoroNa Green in the present study for FLIM *in vitro* and *in situ* (Meyer et al. 2019).

The widely used Na^+-sensitive dye SBFI does only show minor differences in τ and therefore seems to be not suitable for FLIM (Despa et al. 2000). Other Na^+ dyes have been tested for their suitability for FLIM *in vitro* and only to a minor extent *in situ*.

For proper usage in FLIM, the dye of interest needs to meet certain criteria. The sensitivity for Na^+ should be high and the sensitivity for other cations and also changes in pH should be comparatively low. To this extent, usually *in vitro* measurements are performed, in order to get the most basic idea of the properties of the dye (see Fig. 12, Meyer et al. 2019).

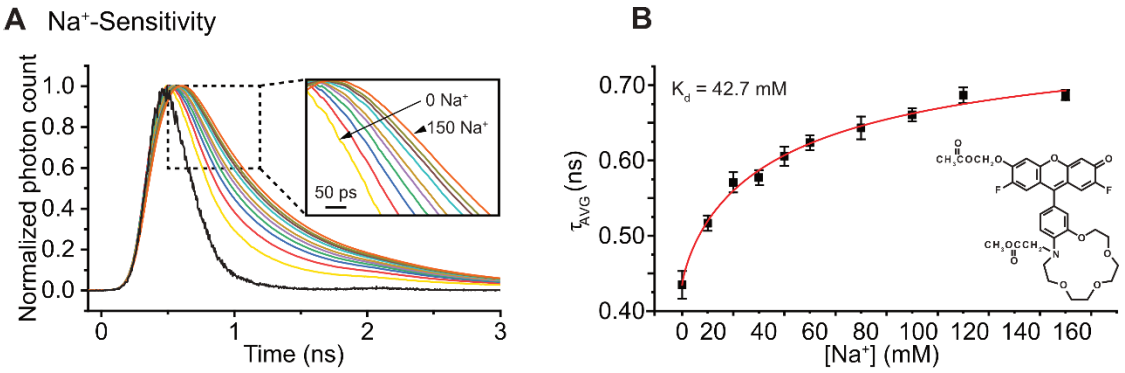

Figure 12: *In vitro* calibration of CoroNa Green. **A** CoroNa Green was calibrated for FLIM *in vitro* with salines containing various $[Na^+]$ ranging from 0 to 150 mM Na^+. Illustrated is the distinct photon distribution, specific to CoroNa Green at the various levels of Na^+. Note: The shift in the decay towards the right side, indicating an increase in τ with increasing $[Na^+]$. **B** The average fluorescence lifetime (τ_{AVG}) is plotted against the $[Na^+]$, revealing a sigmoidal relationship and a K_D of ~47.2 mM. The lifetime raised from ~0.43 ns (unsaturated at 0 Na^+) to ~0.69 ns (saturated at 150 Na^+). The structure of CoroNa Green is depicted in the lower right. Modified and reprinted with permission from Meyer et al. (2019)

CoroNa Green shows high Na^+-sensitivity *in vitro* but with a low dynamic range of ~300 ps and a K_D of 42.7 ± 12.7 mM (Fig. 12, Meyer et al. 2019). During physiological processes not only the Na^+ concentration but also other ions can change. It was shown that e.g. glutamate receptor activation induces changes in intracellular pH in the range of pH 7-7.5 (Kelly et al. 2009, Kelly and Rose 2010). $[K^+]_i$ mirrors the $[Na^+]_i$, and during synaptic transmission Na^+ enters the cell, K^+ consecutively flows out and thereby repolarizes the cellular membrane (Kofuji and Newman 2009). Because of the changes in other ions, the optimal sodium sensitive dye would be insensitive to changes in ions other than sodium. CoroNa Green showed no

significant influence on changes in pH within the range of 6.0 to 8.0 and only a negligible influence of K^+ in the physiological range *in vitro* (30 – 150 mM, Meyer et al. 2019). If a dye is to be used in an intracellular environment, a possible influence of high viscosity needs to be investigated, as the intracellular space is densely packed. *In vitro* this can be done by the addition of different concentrations of dextran, a branched polysaccharide (Zheng et al. 2014). For example a solution with 5% of 50 kD dextran (weight in H_2O) corresponds roughly to the viscosity of blood (Carrasco et al. 1989). For CoroNa the influence of viscosity has been investigated in two different concentrations, unsaturated (0 mM Na^+) and saturated (150 mM Na^+) and no influence of dextran on the τ_{AVG} was found (Meyer et al. 2019). The low dependency on other ions, pH and viscosity makes CoroNa an ideal candidate for further probing in a cell culture environment.

Ion sensitive dyes have been proven to show different sodium sensitivities when used in living cells in comparison to *in vitro* (Langer and Rose 2009). A careful calibration in the cellular preparation of choice is therefore a necessity (Fig. 13).

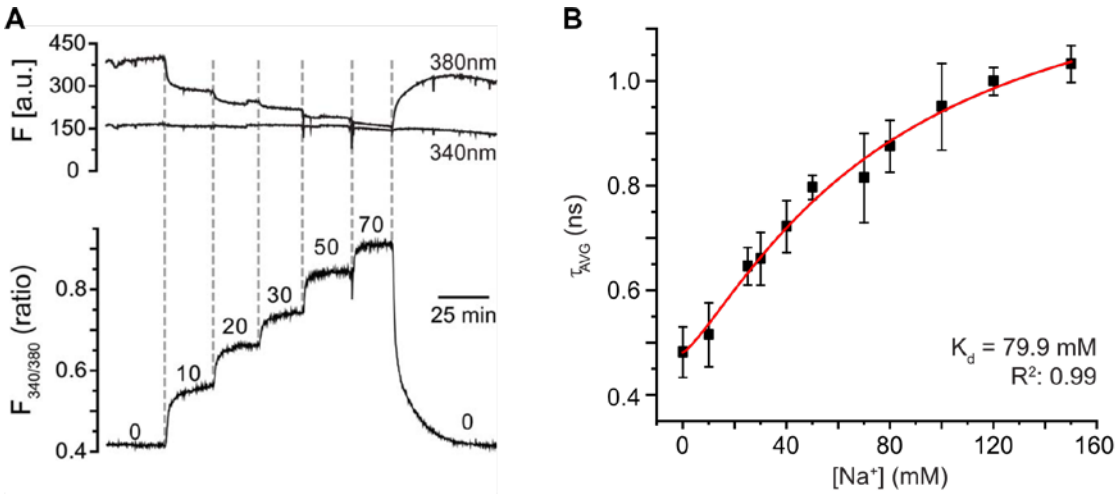

Figure 13: *In* situ sodium calibration. A: Exemplary calibration of SBFI. To promote rapid equilibration of Na^+ in the intra- and extracellular space, the cell membranes were permeabilized with gramicidin (a Na^+-pore) and monensin (a Na^+-/H^+-Exchanger), while inhibiting the NKA with ouabain. Cells were then perfused with 0, 10, 20, 30, 50 and 70 mM Na^+ until a plateau was reached at each stage. The upper graph shows the ratiometric behaviour of the dye SBFI, with the Na^+ insensitive wavelength of 340 nm, and the sensitive wavelength of 380 nm. Below the corresponding ratio (340/380) is plotted over a time course of ~2 hours. **B:** A comparable calibration for CoroNa and FLIM. HEK cells were treated as in A and the photons were counted for 80 s per image. The resulting photon distribution was fitted with a bi-exponential reconvolution fit and the consequent average fluorescence lifetime (τ_{AVG}) was plotted against the [Na^+], revealing a sigmoidal behaviour of CoroNa and a K_D of 79.9 mM. A: reprinted with permission from Karus et al. 2015, B: from Meyer et al. 2019

Sodium can be calibrated using the so called ionophores gramicidin and monensin, by simultaneous inhibition of the NKA with ouabain (Rose and Ransom 1996). Gramicidin is a linear pentadecapeptide, that integrates into the cellular membrane and thereby forms a cation selective pore (Harootunian et al. 1989). The simultaneous addition of monensin results in the additional equilibration of Na^+ as well as H^+, since monensin functions as a Na^+-H^+- exchanger (Levl et al. 1994). Furthermore, the NKA inhibitor ouabain (a cardiac glycoside) is added to inhibit the re-establishment of the Na^+-gradient. After the permeabilization, the preparation is perfused with salines containing different concentrations of Na^+ (see Fig. 13A) until a plateau is reached. Afterwards either the obtained changes in fluorescence intensity or in the case of FLIM the τ_{AVG} values can be plotted against the corresponding Na^+-concentration and the data is fitted (usually with Michaelis-Menten kinetics) to calculate the K_D of the dye and more importantly to quantify Na^+ (Fig. 13B). One key benefit of FLIM in combination with Na^+ indicators is, as the calculation of the $[Na^+]$ relies on the lifetime, that it is always reporting absolute values. Fluorescence intensity measurements can only identify changes in the $[Na^+]_i$, as the baseline fluorescence is variable and can change due to secondary factors like variations in dye concentration or focus (Fig. 14A, B).

To obtain baseline concentration of a certain cell it was up to now needed to adapt a certain technique called *patch-clamp* (Neher and Sakmann 1976) and combine it with bolus-loading. The Patch-clamp technique is famous for its ability to measure changes in membrane potential, but can also be used to dialyse the cell with a certain saline or fluorescent dye (also see Fig. 14A). Bolus-loading, describes the procedure, were a specific form of an indicator dye (e.g. SBFI) is injected into a tissue slice with a fine glass pipette. An esterified form of the dye is used and therefore the dye is membrane permeable. Once inside the cell, ubiquitously expressed esterases detach the esters, rendering the dye cell membrane impermeable and trapped inside of the cell. Then, both techniques were combined: The already bolus stained cell of interest is approached with a very fine glass pipette (tip diameter <1 µm). Once a connection between the cell and the pipette is established, the pipette concentration will determine the cellular concentration. As the concentration inside the pipette is known, the change in baseline upon breakthrough can be quantified and the former baseline concentration can be calculated (Mondragao et al. 2016, Ziemens et al. 2019).

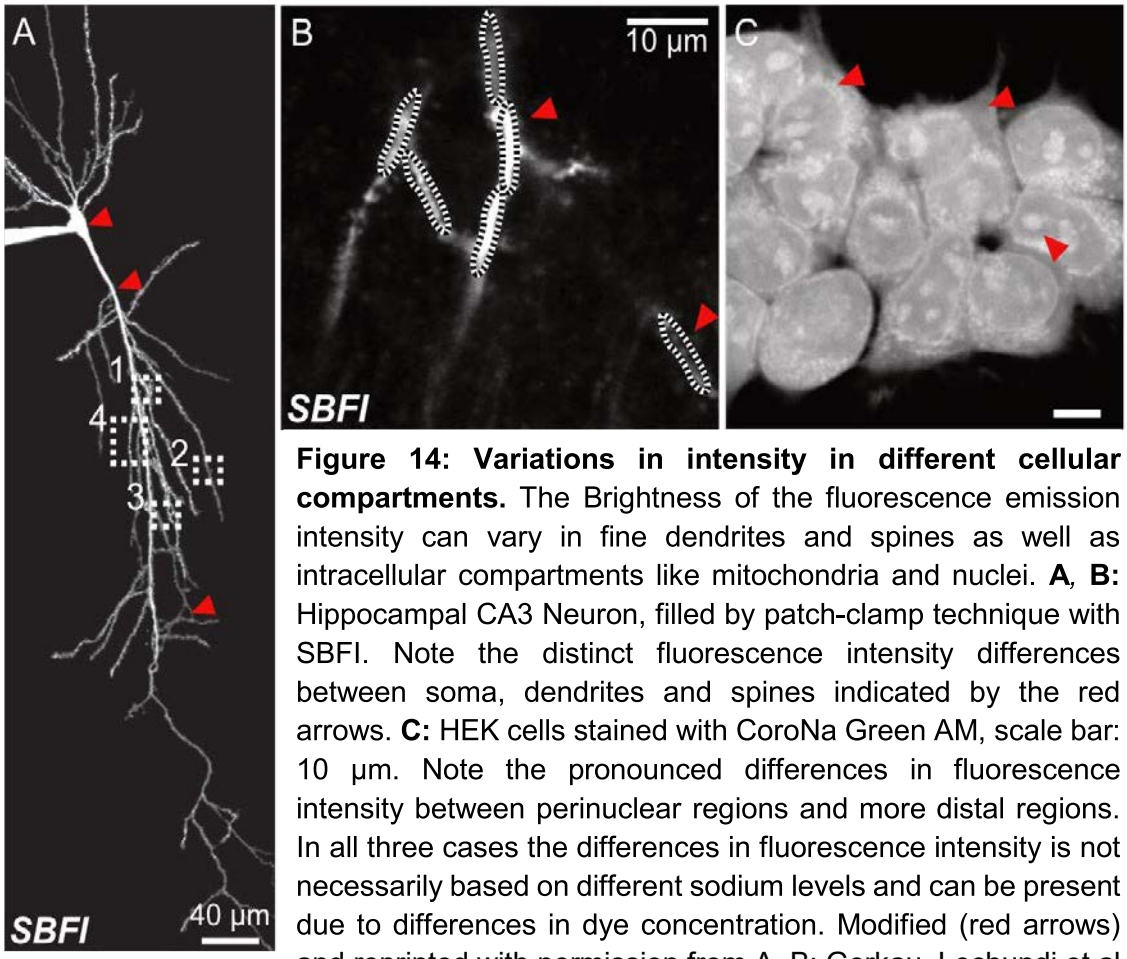

Figure 14: Variations in intensity in different cellular compartments. The Brightness of the fluorescence emission intensity can vary in fine dendrites and spines as well as intracellular compartments like mitochondria and nuclei. **A**, **B:** Hippocampal CA3 Neuron, filled by patch-clamp technique with SBFI. Note the distinct fluorescence intensity differences between soma, dendrites and spines indicated by the red arrows. **C:** HEK cells stained with CoroNa Green AM, scale bar: 10 µm. Note the pronounced differences in fluorescence intensity between perinuclear regions and more distal regions. In all three cases the differences in fluorescence intensity is not necessarily based on different sodium levels and can be present due to differences in dye concentration. Modified (red arrows) and reprinted with permission from A, B: Gerkau, Lechundi et al (2019) and C: Meyer et al (2019).

In contrast, FLIM relies on the intrinsic lifetime of the dye and therefore constantly reports absolute values of the $[Na^+]_i$. In combination with bolus-loading many cells can be observed at once, and their $[Na^+]_i$ under resting conditions can easily be quantified. In the study at hand, I was able for the first time to quantify the $[Na^+]_i$ at ~15 mM in a large number of hippocampal CA1 neurons (> 400 cells), which is in line with previous findings (Meyer, Gerkau et al. submitted)

Another drawback of the aforementioned patch-clamp technique combined with intensity imaging is that it is neither possible to quantify baseline values in fine compartments (like dendrites and spines, Fig. 14B), nor in subcellular areas (like mitochondria or the nucleus, see Fig. 14C). Both caused by the fact, that a difference in fluorescence intensity could also arise from a difference in dye concentration, which is not entirely neglectable. FLIM on the other hand is not influenced by dye concentration differences and therefore represents an ideal tool to study this static processes, as well as differences within the cell.

For Ca^{2+} a compartmentation is described in some subcellular structures, mainly nucleus and mitochondria (Bengtson et al. 2010, Bading 2013). The presence of Na^+ coupled transporter in the mitochondrial membrane (Murphy and Eisner 2009, Parnis et al. 2013) indicate a compartmentation of Na^+ as well and indicates a tight relationship between Na^+-signalling in the soma and comprising other organelles. To evaluate the importance of Na^+-signals in organelles the knowledge about the $[Na^+]$ in the soma as well as in the organelles is of great importance.

In the first part of this study I addressed a possible difference in $[Na^+]_i$ and utilized FLIM with Corona Green in human embryonic kidney (HEK) cells. Here, I found a cytosolic $[Na^+]$ of ~ 18 mM as well as an increased $[Na^+]$ in perinuclear regions of ~27 mM. In contrast nuclear $[Na^+]$ was significantly lower, amounting to ~13 mM (Fig. 15, Meyer et al. 2019).

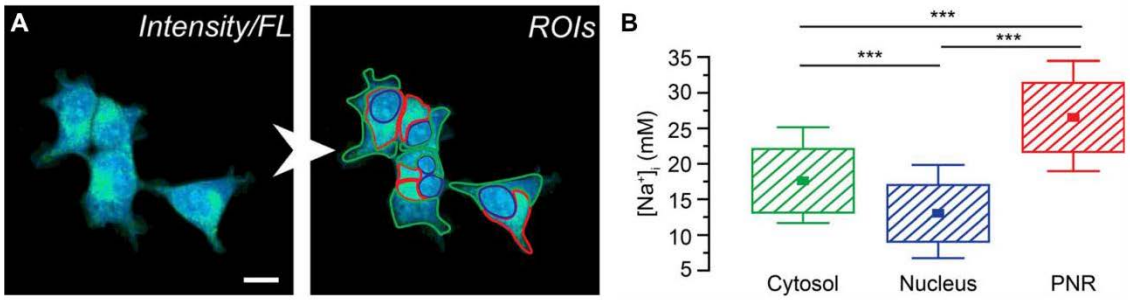

Figure 15: Differences in $[Na^+]$ in cellular subcompartmens are highlighted by FLIM
A Fluorescence lifetime image of CoroNa Green stained HEK-cells. FLIM images are depicted with a colorcode (blue for low Na^+, scaling over green, yellow to red for high Na^+) and brightness indicating for the number of photons collected. On the left, note the clear heterogeneity in the fluorescence lifetime. Right: Regions of interests (ROIs) were drawn for the distinct different areas. **B** Box plots (square: mean; box: SD and whiskers: 95/5 percentile) of the different $[Na^+]_i$ in the different subcellular regions. Note: the decreased $[Na^+]_i$ in the Nucleus and increased $[Na^+]_i$ in perinuclear regions (PNR). Modified and reprinted with permission from Meyer et al. (2019).

9. Limitations of TCSPC and alternative approaches

The major drawback of TCSPC is the long time needed to reach sufficient enough photons for a stable decay calculation, resulting in low temporal resolution. Usually, a minimum threshold of >5000 photons per decay is needed for appropriate fitting conditions. Hence, the collection time needed to construct one single FLIM image is between 50-120 s (Wilms et al. 2006, Hille et al. 2009, Roder and Hille 2014). The counting time is directly dependent on the number of

photons, which can be registered. When imaging biological specimens, the excitation strength and duration are two major limiting factors, both causing phototoxic damage when increased excessively. Concerning TCPSC the overall systems dead time is additionally limiting the photon count. TCSPC electronics usually need ~100 ns of computation time, after registering a photon, a phenomenon called dead time (Patting et al. 2007). When high frequency repetition lasers are used e.g. 80 MHz, only one photon every ~7 excitation pulses can be registered, causing a bias for fast photons as already the first photon will blind the TCSPC electronics for later arriving photons (Becker 2015). This bias is called pulse pile-up and is reducing the measured lifetime when the count-rate is exceeding approx. 1-5% of the laser repetition rate (e.g. 80 Mhz, 4 MCtns/s, Lakowicz 2006). Another important point concerning the count-rate is photon-loss, which describes the number of photons that are not registered, during the dead-time of the TCSPC hardware. Pulse-pile-up and photon loss are two major reasons reducing the dynamic capabilities of FLIM (Becker 2015). One possibility is to use a so-called time-gated approach (Fig. 16A, King et al. 2020). Here only two areas of photons are taken into account, naming the very fast and the slow portion of the photon distribution (Buurman et al. 1992). With this method very high imaging frequencies can be achieved and it was possible to show, that resting baseline Ca^{2+} controls the size and shape of astroglial Ca^{2+}-signals (King et al. 2020).

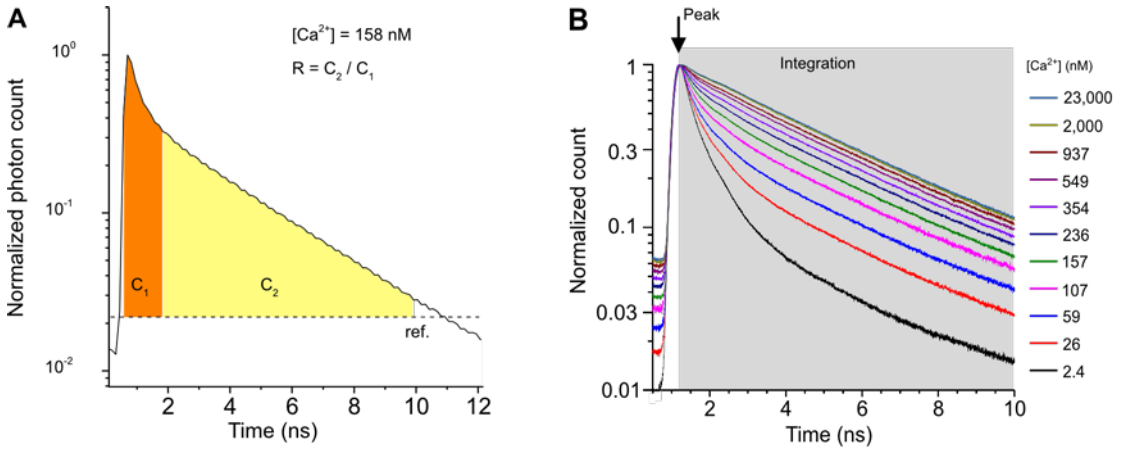

Figure 16: Alternative approaches to utilize TCSPC and measure an intracellular ion concentration A Here the photon distribution of Oregon Green Bapta-2 (OGB-2) was split into two time-gates to characterize the dependence of the lifetime of OGB-2 on Ca^{2+} **B** The photon distribution of Oregon Green Bapta-1 (OGB-1) at different Ca^{2+} concentrations. Instead of two time-gates, integration window is normalized to the peak, resulting in a value that is dependent on Ca^{2+}. Modified and reprinted with permission from A: King et al. (2020) and B: Zheng et al. (2018).

In the first part of this project, I used the same technique to investigate if the aforementioned differences in baseline [Na^+] in different subcellular region may have an impact on sodium dynamics during metabolic inhibition. To this end, CoroNa stained HEK cells were perfused with nominally K^+-free solution, which results in a steep increase in $[Na^+]_i$. Using a variation of the time-gated approach (here termed ratioFLIM) enabled reliable Na^+ quantification and an increase in temporal resolution up to 10 fold. Classical fitting based FLIM (also see Fig. 15) took 80s per image, however with the ratioFLIM approach imaging with a frequency of one image every 8 s was possible. Interestingly, this made a temporal delay between the cytosol and the nucleus (+24 s), as well as perinuclear regions (+40 s) visible (Fig. 17, Meyer et al. 2019).

In summary, I was able to highlight that ratioFLIM is able of measuring changes in [Na^+] on subcellular level, as well as increasing the temporal resolution over classical FLIM several fold.

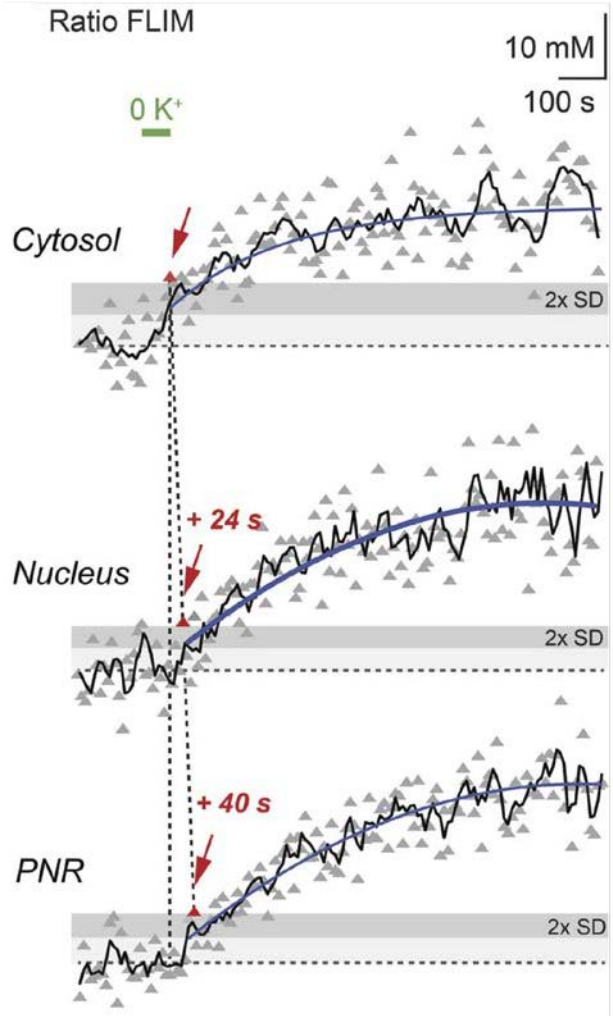

Figure 17: Temporal difference in Na^+-loading highlighted by ratioFLIM. To simulate metabolic inhibition, CoroNa stained HEK cells, were perfused with nominally K^+-free solution for a brief period of 1 min. Changes in [Na^+] were depicted for each of the three analysed compartments. Grey triangles represent individual data points. The first data point exceeding two times standard deviation is indicated with a red arrow and triangle. Note the distinct delay in response in respect to the cytosol (top), of the nucleus (middle, +24 s) and perinuclear regions (bottom, +40 s). Reprinted with permission from (Meyer et al. 2019)

An alternative approach, based on the same principle, is instead of utilizing two or multiple time-gates, integrating the whole photon distribution by the peak photon count (Normalized Total Count, NTC) (Fig. 15B, Zheng et al. 2015). This can result in greater signal stability but is dependent on the lifetime of the observed fluorophore and thereby the shape of the photon distribution. For Oregon Green Bapta-1 and 2 (OGB-1 and OGB-2) it has been shown, that compared to traditional TCSPC, the signal to noise ratio could be drastically improved by up to ~2.5 fold when the photon count is below a reported threshold of 2000 counts (Zheng et al. 2015, King et al. 2020). As the technique relies on the same principles as TCSPC, it suffers from the same problems (like *pulse pile-up* and *photon-loss*) but is able to mask some of them by reducing the error of fitting by several fold. The benefit of the technique results from the proportion between the peak photon count and the overall photon count. If a dye exhibits a relatively long lifetime (For OGB-1 and 2: 0.5 ns to 4 ns, Sagolla et al. 2013, Zheng et al. 2015) the overall photon count and resulting from that, the ratio between the peak photon count and the overall photon count will be relatively stable. In the case of Na^+ all dyes tested so far exhibit lifetimes in the low ns range (~0.5 – 1.5 ns), with lower dynamic range and lower quantum efficiency (Roder and Hille 2014). Additionally, with a short lifetime, the number of slow photons is low and therefore subject to statistical fluctuation, which might reduce the effectivity of the NTC approach.

All of the aforementioned approaches, improve the manageability of low photon numbers. However, the ultimate approach to increase the acquisition speed would be a reduction in the dead time of the detectors and TCSPC hardware. This would result in an increased number of photons that are usable for analysis.

10. rapidFLIM: a novel tool for Na^+ imaging investigated in this study

In the second part of this study, newly developed hybrid photo detectors (HPD) and TCSPC electronics, were used for the first time with Na^+-sensitive indicators in acute brain tissue slices (Meyer, Gerkau et al. submitted). As both devices exhibit extremely low dead-times of combined ~0.6 ns (compared to classic electronics with deadtimes > 80ns), dead-time artefacts can be called nearly inexistent (Michalet et al. 2008, Zadeh et al. 2018, Wahl et al. 2020). Here, the benefits of the newly termed *rapidFLIM* and a possible combination with the sodium sensitive indicator dye ION NaTRIUM Green-2 were elucidated (Meyer, Gerkau et al., submitted)

rapidFLIM is the combination of ultra-low dead-time electronics, drastically reducing the number of lost photons, with an algorithm correcting for a) *pulse-pile-up* (also see chapter 8)

and b) the electrical merging of two consecutive, close photons called *electrical pulse-pile-up* (EPP, see Fig. 18).

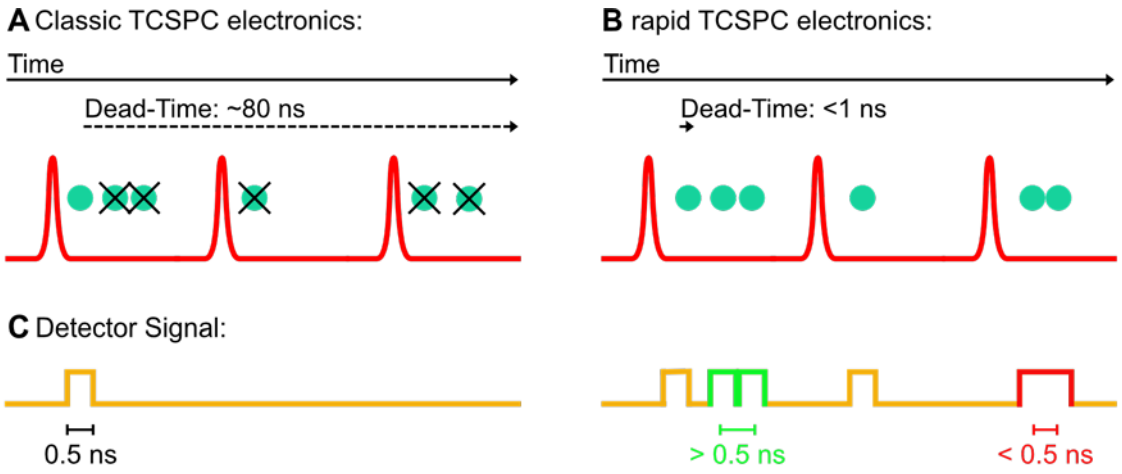

Figure 18: The benefits of rapidFLIM electronics. A Scheme of a typical FLIM recording. Excitation is shown in red, registered photons in green. Here an 80 MHz repetition laser is used for excitation, resulting in an inter-pulse duration of 12.5 ns. Classic TCSPC electronic exhibit a dead-time (time were no photons can be registered) of ~80 ns. Resulting from that, only one photon every ~7 excitation pulses can be registered **B** Rapid TCSPC electronics only have a dead-time of below 1 ns. Thereby, every photon can be registered, rendering dead-time inexistent. **A, B:** The detector signal is shown in yellow. Left: the electrical pulse width of a modern detector is 0.5 ns. Right: If two photon arrive with more than 0.5 ns in between, they are registered as two individual photons. However, if two photons are recorded too close to each other, they are registered as one. This phenomenon is called electrical pulse pile-up (EPP). From Meyer, unpublished

The width of the detector pulse, once a photon is registered is ~0.5 ns with low dead time hybrid photomultiplier detectors (HPDs, see Fig. 18A). When two photons are registered temporarily too close to each other (within 0.5ns) the TCSPC unit will not detect the second photon, as it is within the pulse width of the detector signal (Fig. 18B). This results in an underrepresentation of fast photons and thereby a shift of the photon peak towards slower lifetimes. The present study proposes a correction algorithm that is effectively reducing fitting errors by up to ~50 fold and enables photon count rates of up to 2 photons per excitation cycle (Fig. 18; Meyer, Gerkau et al. submitted). While regular FLIM takes multiple tens of seconds to record enough photons to construct an image, with rapidFLIM and the reduced dead-time it was possible for the first time to speed up the imaging process of $[Na^+]_i$ based on τ up to 0.5 Hz at full frame resolution and exemplarily up to 2 Hz at reduced resolution (Meyer, Gerkau et al. submitted).

The first step was to test ING-2's changes in fluorescence lifetime upon changing the sodium concentration. As mentioned before (see chapter 8, Fig. 12) this is typically done in an *in vitro* environment, as the experimental parameters are easily controllable. Here, ING-2's fluorescence lifetime changed from 0.361 ± 0.040 ps in the absence of Na^+ (0 mM Na^+) to 1.477 ± 0.023 ps when it was saturated with Na^+ (150 mM Na^+). Additionally, the reaction to other parameters like K^+, pH and viscosity showed no significant dependence (Meyer, Gerkau et al. submitted). It was reported, that sodium dyes and in particular ANG-2, which is the predecessor of ING-2, would be influenced by the ionophore monensin (also see chapter 6, Yurinskaya et al. 2020). Therefore, the impact of monensin and gramicidin, which are both used in this study were validated. In our experimental hands, no significance dependence on τ_{AVG} was found (Meyer, Gerkau et al. submitted).

Chemical indicator dyes change their properties when they are used in a cellular environment (also see Chapter 8, Langer and Rose 2009). Therefore, ING-2 was calibrated for the first time *in situ* simultaneously for fluorescence lifetime and intensity. For this purpose, organotypic slice culture (for detailed methods see Gerkau, Lerchundi et al. 2019 and Meyer, Gerkau et al. submitted) was loaded with ING-2 AM and perfused with solutions containing various Na^+-concentrations. A strong dependence of τ_{AVG} to the $[Na^+]$ could be observed, ranging from ~0.5 ns at 0 mM to ~1.5 ns at 150 mM $[Na^+]_i$ and a change in fluorescence intensity ($\Delta F/F_0$) of around three fold. As aforementioned, the baseline is classically identified using single cells (Mondragao et al. 2016, Ziemens et al. 2019). With the rapidFLIM method proposed in this study, it was possible for the first time to quantify the $[Na^+]_i$ in a large number of hippocampal CA1 neurons (>400 neurons), supporting the previously found concentration of ~15 mM (Meyer, Gerkau et al. submitted).

Next this study tested the suitability of rapidFLIM to quantify swift changes in $[Na^+]_i$. To this extent, I applied 1 mM glutamate for 10 s via global perfusion (not shown) as well as for 100 ms, via a fine glass pipette (Fig. 19A). Utilizing the novel rapidFLIM approach we were able to record images at 0.5 Hz full frame with a resolution of 512 x 512 pixels, showing a transient increase in $[Na^+]_i$ upon glutamate application, which is in line with previous findings (Fig. 19B; Meyer, Gerkau et al. submitted). Comparing global with local signals, a significant increase in amplitude was visible, that in both cases decayed back to comparable baseline values (Fig. 19C). However, while the peak and rise of the global signal was clearly visible, the rising phase of the local signal was faster than the full-frame temporal resolution (Fig. 19B). To this extent, the pressure application of glutamate (100ms) was exemplary repeated at a reduced frame size of 56 x 56 pixel. At this reduced spatial resolution, it was possible to record images at 2 Hz, visualizing not only the peak, but also the rise of the glutamate induced Na^+-transient (Meyer, Gerkau et al., submitted).

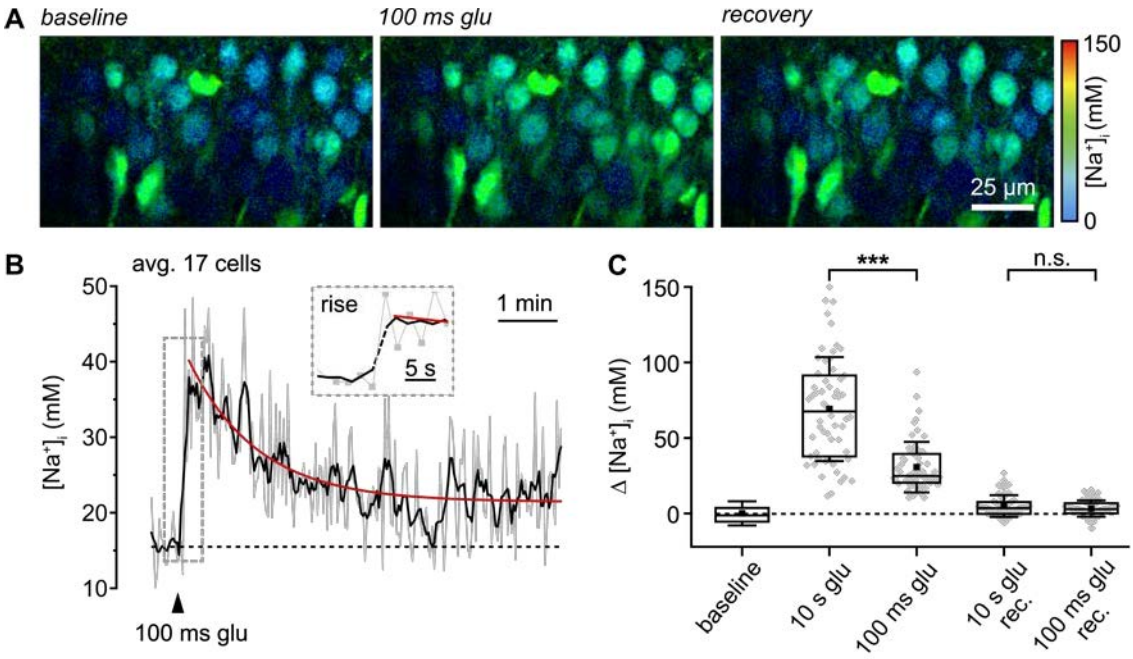

Figure 19: Induced glutamate transients visualized with rapidFLIM at 0.5 Hz. A: An acute hippocampal slice was stained with ING-2. Depicted is an experiment were the frame size was 512 x 512 pixels and the imaging frame rate was 1 Hz. To collect enough photons for stable lifetime calculation a binning of 2 frames was applied, resulting in a temporal resolution of 0.5 Hz. **B:** Same Experiment as in (A) showing the corresponding average lifetime trace (τ_{AVG}). Mean of cells (17) is depicted in grey, a rolling average (5 pt) of the mean in black. Red line represents a monoexponential fit of the recovery phase. Inset shows the same experiment at higher temporal magnification. **C:** Box plots showing means (square), median (line), SD (box), and 25/75 percentiles (whiskers) of peak changes in $[Na^+]_i$ in response to global as well as local glutamate application and upon recovery after 5-10 minutes for both conditions. Grey diamonds are single data points. A Mann-Whitney-test was used for statistical comparison. ***: $p<0.001$. Modified and reprinted with permission from Meyer, Gerkau et al. submitted.

According to the annually WHO-health-report, cardiovascular diseases and especially stroke are the most common cause of death in the world. But its most basic effects on the brain are still to be explored. It was shown that stroke is leading to post infarct depolarization (PID) waves of Na^+ *in vivo* (Gerkau et al. 2018), accompanied by severe cellular swelling. The latter drastically hinders the possibility of imaging experiments (Allen et al. 2004, Kimelberg 2005). One of the key benefits of FLIM is the insensitivity to changes in the dye concentration and thereby its robustness against secondary factors like cellular swelling, shift in focus or dye lost (Becker 2015). In this study we elucidate the capabilities of FLIM to measure at challenging conditions were aforementioned secondary factors can occur. To this extent we used ING-2

stained acute tissue slices and exposed them with glucose-free saline containing 5 mM sodium azide ($NaN_{3)}$ and 2 mM 2-deoxyglucose (2-DG) for 2 minutes (mild), 5 minutes (moderate) and 5 minutes with doubled concentrations (severe) to mimic various degrees of metabolic inhibition. Using this approach we were able to show that rapidFLIM based measurements showed increasing amplitudes in $[Na^+]_i$ with increasing metabolic stress. However, intensity based measurement did not exceed the amplitudes induced by mild ischemia, when modest or even severe induction was used (Meyer, Gerkau et al., submitted)

With rapidFLIM and ING-2 it was possible for the first time to dynamically measure the influence of metabolic inhibition on the $[Na^+]_i$ even under severe cellular stress accompanied by substantial cell swelling (Fig. 20A; Meyer, Gerkau et al. submitted).

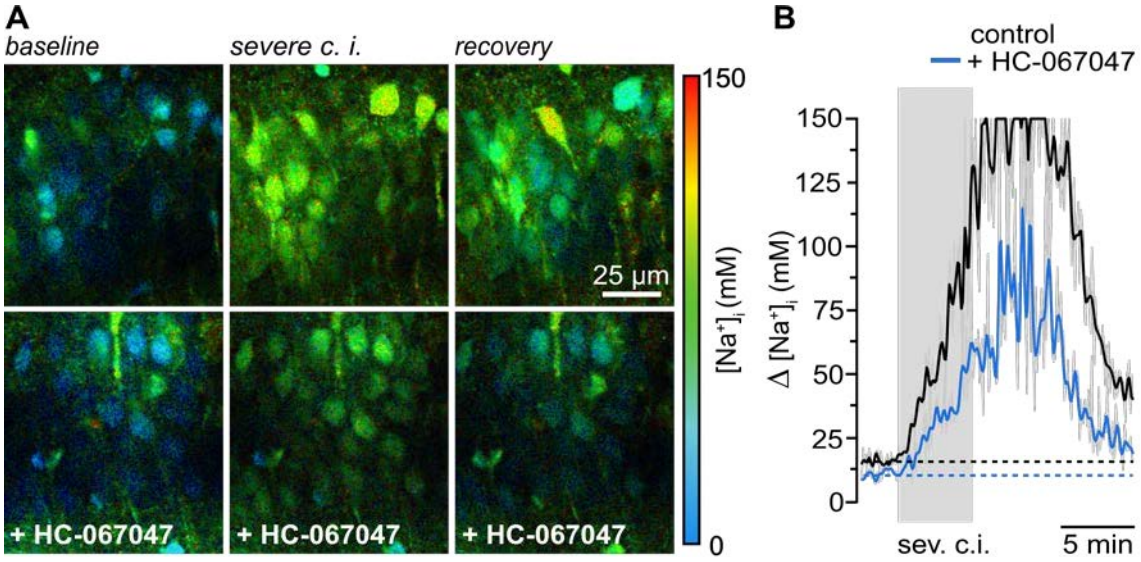

Figure 20: Quantification of A: An acute hippocampal tissue slice was stained with ING-2 and treated with severe chemical ischemia for 5 min (top). In a subset of experiments HC-067047, a blocker for TRPV4 channels was added (bottom). Fluorescence lifetime images are illustrated in a color-coded manner with blue indicating for low, red indicating for high Na^+ and brightness indicating for photon numbers. The color-code is depicted on the right. **B:** Same Experiment as in (A) showing the corresponding average lifetime trace (τ_{AVG}). The average of all neurons in the field of view is depicted in grey, a rolling average (5 pt) of these cells in black for control conditions and blue for conditions where HCC-067047 was added. Modified and reprinted with permission from Meyer, Gerkau et al. submitted.

The cause for cellular swelling is yet to be unravelled. It was shown, that neuronal swelling is dependent on Na^+ and Cl^- but independent of Ca^{2+} and is facilitated by the voltage-gated chloride channel SLC26A11 (Rungta, Choi et al. 2015). One influx pathway for Na^+ is the activation of NMDA-receptors under ischemic conditions, which accounts to ~50% in hippocampal CA1 neurons (Gerkau et al. 2018). Additionally, the temperature-sensitive cation channel TRPV4 (Transient Receptor Potential Vanilloid 4) might be a possible candidate for

further sodium loading as it was identified as one of the main causes for brain oedema (Hoshi et al. 2018). In the present study it was shown for the first time that, blockage of the TRPV4 reduces sodium loads by almost 50% under severe ischemic conditions (Fig. 20B) and furthermore inhibits the accompanied swelling completely (Meyer, Gerkau et al., submitted).

11. Concluding remarks and Outlook:

Over the last decades the measurement of Na^+-signalling in neurons and astrocytes was widely established (Rose et al. 1997, Rose 2003, Kelly et al. 2009, Langer et al. 2012, Gerkau et al. 2017, Ziemens et al. 2019). This study contributed to both fields: I: by elucidating a relationship between energy demand and global as well as local Na^+-signals in neurons (Gerkau et al. 2019) and II: by detecting a possible pathway for seizure exacerbation under pathophysiological conditions, through gap junction uncoupling in astrocytes (Onodera et al. 2021).

In previous studies mainly intensity based imaging was used to investigate changes in intracellular ion and metabolite concentration. Quantification in these cases can be impaired as the intensity is strongly dependent on factors like changes in dye concentration or focus. Both can occur during pathophysiological conditions (e.g. during stroke) preventing proper quantification. In my work a new method that is independent of aforementioned secondary factors was proposed. By combining FLIM with Na^+-sensitive indicators, I was able to elucidate subcellular compartmentation of HEK-cells (Meyer et al. 2019) as well as quantify $[Na^+]_i$ under severe metabolic stress, which is accompanied by major cellular swelling in neurons (Meyer, Gerkau et al., submitted).

While this study was able to show subcellular compartmentation of Na^+ in HEK cells, a possible compartmentation in neurons and astrocytes is still elusive. Here, the quantitative knowledge of the $[Na^+]_i$ is especially important as a reversal of transporters that are Na^+-dependent, may directly affect neurotransmission as well as other ion concentrations (e.g. Ca^{2+} via the NCX). These confined environments are difficult to address, as they have low volumes and therefore usually low dye concentrations.

I believe, that the proposed rapidFLIM in this study, will pave the way for a broad number of applications and most importantly enable the improved measurement of ions and metabolites with dim fluorescent probes in the future.

Contributions to the submitted manuscript and publications:

12.1 Submitted manuscript:

Publications are sorted chronologically, starting by the newest submitted manuscript and followed by the publications. For reasons of copyright protection, the published version of this dissertation does not contain reprints of the articles.

Pages 33-73:

rapidFLIM for dynamic lifetime-imaging with dim fluorophores at unprecedented speed

Jan Meyer*, Niklas J. Gerkau*, Karl W. Kafitz, Matthias Patting, Fabian Jolmes and Christine R. Rose

Shared first authorship

Nature Methods (submitted 2021)

Impact factor 2019/2020: 30.822

I performed:

- All measurements depicted in figures 3 and 4, supplement figures 1 and 3
- All analysis for FLIM data depicted in figures 2-6 and supplement figures 1-3
- Initial draft of the introduction, methods and results

I contributed to:

- The measurements depicted in figure 2 and supplement figure 2
- The conceptualization and methodology of the study
- Drafting and revision of the manuscript and figures
- Interpretation of data

12.2 Publications:

Pages 74-133:

Exacerbation of epilepsy by astrocyte alkalization and gap junction uncoupling.

Mariko Onodera**, Jan Meyer**, Kota Furukawa, Yuichi Hiraoka, Tomomi Aida, Kohichi Tanaka, Kenji F. Tanaka, Christine R. Rose, and Ko Matsui

Journal of Neuroscience (2021)

Impact factor (2021 not available), 2019: 5.673

I contributed to:

- Conceptualization and measurement of the data in Figure 1.
- Analysis of the data in Figure 1.

Pages 134-146:

Quantitative determination of cellular [Na+]by fluorescence lifetime imaging with CoroNaGreen

Jan Meyer, Verena Untiet, Christoph Fahlke, Thomas Gensch, and Christine R. Rose

Journal of General Physiology (2019)

Impact factor 2019: 3.628

I performed:

- All experiments and analysis
- First draft of the methods and results

I contributed to:

- Design and conceptualization of research
- Interpretation of the data
- Review and editing of the manuscript

Pages 147-165:

Relation between activity-induced intracellular sodium transients and ATP dynamics in mouse hippocampal neurons.

Niklas J. Gerkau, Rodrigo Lerchundi, Joel S. E. Nelson, Marina Lantermann , **Jan Meyer**,

Johannes Hirrlinger and Christine R. Rose

The Journal of Physiology (2019)

Impact factor 2019: 4.547

I contributed to:

- Conceptualization of the study
- Drafting and revision of the manuscript and figures

13. References:

Algar, W. R., N. Hildebrandt, S. S. Vogel and I. L. Medintz (2019). "FRET as a biomolecular research tool — understanding its potential while avoiding pitfalls." Nature Methods **16**(9): 815-829.

Allen, N. J. and B. A. Barres (2009). "Neuroscience: Glia - more than just brain glue." Nature **457**(7230): 675-677.

Allen, N. J., D. J. Rossi and D. Attwell (2004). "Sequential release of GABA by exocytosis and reversed uptake leads to neuronal swelling in simulated ischemia of hippocampal slices." Journal of Neuroscience **24**(15): 3837-3849.

Araque, A., V. Parpura, R. P. Sanzgiri and P. G. Haydon (1999). "Tripartite synapses: glia, the unacknowledged partner." Trends in neurosciences **22**(5): 208-215.

Bading, H. (2013). "Nuclear calcium signalling in the regulation of brain function." Nat Rev Neurosci **14**(9): 593-608.

Bannister, N. J. and A. U. Larkman (1995). "Dendritic morphology of CA1 pyramidal neurones from the rat hippocampus: I. Branching patterns." The Journal of Comparative Neurology **360**(1): 150-160.

Barres, B. A. (2008). "The Mystery and Magic of Glia: A Perspective on Their Roles in Health and Disease." Neuron **60**(3): 430-440.

Bear, M. F., B. W. Connors and M. A. Paradiso (2008). Neurowissenschaften: Ein grundlegendes Lehrbuch für Biologie, Medizin und Psychologie, Springer-Verlag.

Becker, W. (2012). "Fluorescence lifetime imaging–techniques and applications." Journal of microscopy **247**(2): 119-136.

Becker, W. (2015). Advanced Time-Correlated Single Photon Counting Applications. Berlin, Springer.

Bellot-Saez, A., O. Kékesi, J. W. Morley and Y. Buskila (2017). "Astrocytic modulation of neuronal excitability through K+ spatial buffering." Neuroscience & Biobehavioral Reviews **77**: 87-97.

Ben-Ari, Y. (2014). "The GABA excitatory/inhibitory developmental sequence: a personal journey." Neuroscience **279**: 187-219.

Ben-Ari, Y., I. Khalilov, K. T. Kahle and E. Cherubini (2012). "The GABA excitatory/inhibitory shift in brain maturation and neurological disorders." Neuroscientist **18**(5): 467-486.

Bengtson, C. P., H. E. Freitag, J.-M. Weislogel and H. Bading (2010). "Nuclear Calcium Sensors Reveal that Repetition of Trains of Synaptic Stimuli Boosts Nuclear Calcium Signaling in CA1 Pyramidal Neurons." Biophysical Journal **99**(12): 4066-4077.

Billups, D., M.-C. Marx, I. Mela and B. Billups (2013). "Inducible presynaptic glutamine transport supports glutamatergic transmission at the calyx of Held synapse." Journal of Neuroscience **33**(44): 17429-17434.

Bischof, H., M. Rehberg, S. Stryeck, K. Artinger, E. Eroglu, M. Waldeck-Weiermair, B. Gottschalk, R. Rost, A. T. Deak, T. Niedrist, N. Vujic, H. Lindermuth, R. Prassl, B. Pelzmann, K. Groschner, D. Kratky, K. Eller, A. R. Rosenkranz, T. Madl, N. Plesnila, W. F. Graier and R. Malli (2017). "Novel genetically encoded fluorescent probes enable real-time detection of potassium in vitro and in vivo." Nat Commun **8**(1): 1422.

Blaustein, M. P. and W. J. Lederer (1999). "Sodium/calcium exchange: its physiological implications." Physiological reviews **79**(3): 763-854.

Bröer, S. and N. Brookes (2001). "Transfer of glutamine between astrocytes and neurons." Journal of neurochemistry **77**(3): 705-719.

Bushong, E. A., M. E. Martone, Y. Z. Jones and M. H. Ellisman (2002). "Protoplasmic astrocytes in CA1 stratum radiatum occupy separate anatomical domains." Journal of Neuroscience **22**(1): 183-192.

Buurman, E. P., R. Sanders, A. Draaijer, H. C. Gerritsen, J. J. F. Van Veen, P. M. Houpt and Y. K. Levine (1992). "Fluorescence lifetime imaging using a confocal laser scanning microscope." Scanning **14**(3): 155-159.

Callaway, J. C. and W. N. Ross (1997). "Spatial distribution of synaptically activated sodium concentration changes in cerebellar Purkinje neurons." J Neurophysiol **77**(1): 145-152.

Carrasco, F., E. Chornet, R. P. Overend and J. Costa (1989). "A generalized correlation for the viscosity of dextrans in aqueous solutions as a function of temperature, concentration, and molecular weight at low shear rates." Journal of Applied Polymer Science **37**(8): 2087-2098.

Cauller, L. and B. Connors (1994). "Synaptic physiology of horizontal afferents to layer I in slices of rat SI neocortex." The Journal of Neuroscience **14**(2): 751-762.

Chaudhry, F. A., R. J. Reimer and R. H. Edwards (2002). "The glutamine commute: take the N line and transfer to the A." The Journal of cell biology **157**(3): 349.

Danbolt, N. C. (2001). "Glutamate uptake." Progress in Neurobiology **65**(1): 1-105.

Deitmer, J. W. and C. R. Rose (1996). "pH regulation and proton signalling by glial cells." Progress in neurobiology **48**(2): 73-103.

Denk, W., J. Strickler and W. Webb (1990). "Two-photon laser scanning fluorescence microscopy." Science **248**(4951): 73-76.

Denk, W., M. Sugimori and R. Llinas (1995). "Two types of calcium response limited to single spines in cerebellar Purkinje cells." Proceedings of the National Academy of Sciences **92**(18): 8279-8282.

Denk, W. and K. Svoboda (1997). "Photon upmanship: why multiphoton imaging is more than a gimmick." Neuron **18**(3): 351-357.

Denk, W., R. Yuste, K. Svoboda and D. W. Tank (1996). "Imaging calcium dynamics in dendritic spines." Current opinion in neurobiology **6**(3): 372-378.

Despa, S., P. Steels and M. Ameloot (2000). "Fluorescence lifetime microscopy of the sodium indicator sodium-binding benzofuran isophthalate in HeLa cells." Anal Biochem **280**(2): 227-241.

Elston, G. N. (2003). "Cortex, Cognition and the Cell: New Insights into the Pyramidal Neuron and Prefrontal Function." Cerebral Cortex **13**(11): 1124-1138.

Eroglu, C. and B. A. Barres (2010). "Regulation of synaptic connectivity by glia." Nature **468**(7321): 223-231.

Fleidervish, I. A., N. Lasser-Ross, M. J. Gutnick and W. N. Ross (2010). "Na+ imaging reveals little difference in action potential–evoked Na+ influx between axon and soma." Nature neuroscience **13**(7): 852.

García-Marín, V., P. García-López and M. Freire (2007). "Cajal's contributions to glia research." Trends in Neurosciences **30**(9): 479-487.

Gerkau, N. J., R. Lerchundi, J. S. E. Nelson, M. Lantermann, J. Meyer, J. Hirrlinger and C. R. Rose (2019). "Relation between activity-induced intracellular sodium transients and ATP dynamics in mouse hippocampal neurons." J Physiol **597**(23): 5687-5705.

Gerkau, N. J., C. Rakers, S. Durry, G. C. Petzold and C. R. Rose (2017). "Reverse NCX Attenuates Cellular Sodium Loading in Metabolically Compromised Cortex." Cereb Cortex: 1-17.

Gerkau, N. J., C. Rakers, S. Durry, G. C. Petzold and C. R. Rose (2018). "Reverse NCX Attenuates Cellular Sodium Loading in Metabolically Compromised Cortex." Cereb Cortex **28**(12): 4264-4280.

Gerkau, N. J., C. Rakers, G. C. Petzold and C. R. Rose (2017). "Differential effects of energy deprivation on intracellular sodium homeostasis in neurons and astrocytes." J Neurosci Res **95**(11): 2275-2285.

Golgi, C. (1870). "Sulla sostanza connettiva del cervello (nevroglia)." Rendiconti del R Instituto Lombardo di Scienze e Lettere **3**: 275-277.

Golgi, C. (1885). Sulla fina anatomia degli organi centrali del sistema nervoso, S. Calderini.

Haack, N., S. Durry, K. W. Kafitz, M. Chesler and C. Rose (2015). "Double-barreled and Concentric Microelectrodes for Measurement of Extracellular Ion Signals in Brain Tissue." Journal of Visualized Experiments(103).

Halassa, M. M., T. Fellin and P. G. Haydon (2007). "The tripartite synapse: roles for gliotransmission in health and disease." Trends in molecular medicine **13**(2): 54-63.

Hanisch, U. K. and H. Kettenmann (2007). "Microglia: active sensor and versatile effector cells in the normal and pathologic brain." Nat Neurosci **10**(11): 1387-1394.

Harootunian, A., J. Kao, B. Eckert and R. Tsien (1989). "Fluorescence ratio imaging of cytosolic free Na+ in individual fibroblasts and lymphocytes." Journal of Biological Chemistry **264**(32): 19458-19467.

Harris, K. M. (1999). "Structure, development, and plasticity of dendritic spines." Current Opinion in Neurobiology **9**(3): 343-348.

Helmchen, F. and W. Denk (2005). "Deep tissue two-photon microscopy." Nature Methods **2**(12): 932-940.

Hertz, L., R. Dringen, A. Schousboe and S. R. Robinson (1999). "Astrocytes: glutamate producers for neurons." Journal of neuroscience research **57**(4): 417-428.

Hille, C., M. Lahn, H. G. Lohmannsroben and C. Dosche (2009). "Two-photon fluorescence lifetime imaging of intracellular chloride in cockroach salivary glands." Photochemical & photobiological sciences **8**(3): 319-327.

Hirase, H., L. Qian, P. Barthó and G. Buzsáki (2004). "Calcium dynamics of cortical astrocytic networks in vivo." PLoS Biol **2**(4): e96.

Hoshi, Y., K. Okabe, K. Shibasaki, T. Funatsu, N. Matsuki, Y. Ikegaya and R. Koyama (2018). "Ischemic Brain Injury Leads to Brain Edema via Hyperthermia-Induced TRPV4 Activation." The Journal of Neuroscience **38**(25): 5700-5709.

Imamura, H., K. P. Huynh Nhat, H. Togawa, K. Saito, R. Iino, Y. Kato-Yamada, T. Nagai and H. Noji (2009). "Visualization of ATP levels inside single living cells with fluorescence resonance energy transfer-based genetically encoded indicators." Proceedings of the National Academy of Sciences **106**(37): 15651-15656.

Jablonski, A. (1933). "Efficiency of Anti-Stokes Fluorescence in Dyes." Nature **131**(3319): 839-840.

Jabłoński, A. (1935). "Über den mechanismus der Photolumineszenz von Farbstoffphosphoren." Zeitschrift für Physik **94**(1-2): 38-46.

Jaffe, D. B., D. Johnston, N. Lasser-Ross, J. E. Lisman, H. Miyakawa and W. N. Ross (1992). "The spread of Na+ spikes determines the pattern of dendritic Ca2+ entry into hippocampal neurons." Nature **357**(6375): 244-246.

Karus, C., N. J. Gerkau and C. R. Rose (2017). "Differential Contribution of GLAST and GLT-1 to Network Sodium Signaling in the Early Postnatal Hippocampus." OM&P **3**(3, 4): 71-83.

Karus, C., M. A. Mondragao, D. Ziemens and C. R. Rose (2015). "Astrocytes restrict discharge duration and neuronal sodium loads during recurrent network activity." Glia **63**(6): 936-957.

Kazmierczak, J., S. Kempe and B. Kremer (2013). "Calcium in the early evolution of living systems: a biohistorical approach." Current Organic Chemistry **17**(16): 1738-1750.

Kelly, T., K. W. Kafitz, C. Roderigo and C. R. Rose (2009). "Ammonium-evoked alterations in intracellular sodium and pH reduce glial glutamate transport activity." Glia **57**(9): 921-934.

Kelly, T. and C. R. Rose (2010). "Ammonium influx pathways into astrocytes and neurones of hippocampal slices." J Neurochem **115**(5): 1123-1136.

Kettenmann, H., K. H. Backus and M. Schachner (1984). "Aspartate, glutamate and gamma-aminobutyric acid depolarize cultured astrocytes." Neurosci Lett **52**(1-2): 25-29.

Kimelberg, H. K. (2005). "Astrocytic swelling in cerebral ischemia as a possible cause of injury and target for therapy." Glia **50**(4): 389-397.

King, C. M., K. Bohmbach, D. Minge, A. Delekate, K. Zheng, J. Reynolds, C. Rakers, A. Zeug, G. C. Petzold, D. A. Rusakov and C. Henneberger (2020). "Local Resting Ca(2+) Controls the Scale of Astroglial Ca(2+) Signals." Cell Rep **30**(10): 3466-3477 e3464.

Kirischuk, S., L. Héja, J. Kardos and B. Billups (2016). "Astrocyte sodium signaling and the regulation of neurotransmission." Glia **64**(10): 1655-1666.

Kirischuk, S., V. Parpura and A. Verkhratsky (2012). "Sodium dynamics: another key to astroglial excitability?" Trends Neurosci **35**(8): 497-506.

Kofuji, P. and E. A. Newman (2009). Regulation of potassium by glial cells in the centralnervous system. Astrocytes in (patho) physiology of the nervous system, Springer**:** 151-175.

Lakowicz, J. R. (2006). Principles of fluorescence spectroscopy. New York, Springer.

Langer, J. and C. R. Rose (2009). "Synaptically induced sodium signals in hippocampal astrocytes in situ." The Journal of physiology **587**(24): 5859-5877.

Langer, J., J. Stephan, M. Theis and C. R. Rose (2012). "Gap junctions mediate intercellular spread of sodium between hippocampal astrocytes in situ." Glia **60**(2): 239-252.

Lerchundi, R., K. W. Kafitz, M. Farfers, F. Beyer, N. Huang and C. R. Rose (2019). "Imaging of Intracellular ATP in Organotypic Tissue Slices of the Mouse Brain using the FRET-based Sensor ATeam1.03YEMK." J Vis Exp(154).

Levl, A. J., C. O. Lee and P. Brooksby (1994). "Properties of the Fluorescent Sodium Indicator "SBFI" in Rat and Rabbit Cardiac Myocytes." Journal of Cardiovascular Electrophysiology **5**(3): 241-257.

Lichtman, J. W. and J.-A. Conchello (2005). "Fluorescence microscopy." Nature Methods **2**(12): 910-919.

Lin, M. Z. and M. J. Schnitzer (2016). "Genetically encoded indicators of neuronal activity." Nat Neurosci **19**(9): 1142-1153.

Liu, X. B., D. Y. Lin, W. Becker, J. J. Niu, B. Yu, L. W. Liu and J. L. Qu (2019). "Fast fluorescence lifetime imaging techniques: A review on challenge and development." Journal of Innovative Optical Health Sciences **12**(5): 1930003.

Martinez-Hernandez, A., K. P. Bell and M. D. Norenberg (1977). "Glutamine synthetase: glial localization in brain." Science **195**(4284): 1356-1358.

McKenna, M. C. (2007). "The glutamate-glutamine cycle is not stoichiometric: Fates of glutamate in brain." Journal of neuroscience research **85**(15): 3347-3358.

Meier, S. D., K. W. Kafitz and C. R. Rose (2008). "Developmental profile and mechanisms of GABA-induced calcium signaling in hippocampal astrocytes." Glia **56**(10): 1127-1137.

Meyer, J., V. Untiet, C. Fahlke, T. Gensch and C. R. Rose (2019). "Quantitative determination of cellular [Na^+] by fluorescence lifetime imaging with CoroNaGreen." J Gen Physiol **151**(11): 1319-1331.

Michalet, X., A. Cheng, J. Antelman, M. Suyama, K. Arisaka and S. Weiss (2008). "Hybrid photodetector for single-molecule spectroscopy and microscopy." Proc SPIE Int Soc Opt Eng **6862**: 68620F.

Minta, A. and R. Y. Tsien (1989). "Fluorescent indicators for cytosolic sodium." J Biol Chem **264**(32): 19449-19457.

Mondragao, M. A., H. Schmidt, C. Kleinhans, J. Langer, K. W. Kafitz and C. R. Rose (2016). "Extrusion versus diffusion: mechanisms for recovery from sodium loads in mouse CA1 pyramidal neurons." J Physiol **594**(19): 5507-5527.

Murphy, E. and D. A. Eisner (2009). "Regulation of Intracellular and Mitochondrial Sodium in Health and Disease." Circulation Research **104**(3): 292-303.

Nägerl, U. V., K. I. Willig, B. Hein, S. W. Hell and T. Bonhoeffer (2008). "Live-cell imaging of dendritic spines by STED microscopy." Proceedings of the National Academy of Sciences **105**(48): 18982-18987.

Nedergaard, M. and U. Dirnagl (2005). "Role of glial cells in cerebral ischemia." Glia **50**(4): 281-286.

Neher, E. (2012). "Introduction: regulated exocytosis." Cell Calcium **52**(3-4): 196-198.

Neher, E. and B. Sakmann (1976). "Single-channel currents recorded from membrane of denervated frog muscle fibres." Nature **260**(5554): 799-802.

Nimchinsky, E. A., B. L. Sabatini and K. Svoboda (2002). "Structure and function of dendritic spines." Annu Rev Physiol **64**: 313-353.

Oberheim, N. A., T. Takano, X. Han, W. He, J. H. Lin, F. Wang, Q. Xu, J. D. Wyatt, W. Pilcher and J. G. Ojemann (2009). "Uniquely hominid features of adult human astrocytes." Journal of Neuroscience **29**(10): 3276-3287.

Ona-Jodar, T., N. J. Gerkau, S. Sara Aghvami, C. R. Rose and V. Egger (2017). "Two-Photon Na(+) Imaging Reports Somatically Evoked Action Potentials in Rat Olfactory Bulb Mitral and Granule Cell Neurites." Front Cell Neurosci **11**: 50.

Onodera, M., J. Meyer, K. Furukawa, Y. Hiraoka, T. Aida, K. Tanaka, K. F. Tanaka, C. R. Rose and K. Matsui (2021). "Exacerbation of epilepsy by astrocyte alkalization and gap junction uncoupling." J Neurosci.

Orlowski, J. and S. Grinstein (1997). "Na+/H+Exchangers of Mammalian Cells." Journal of Biological Chemistry **272**(36): 22373-22376.

Paluzzi, S., S. Alloisio, S. Zappettini, M. Milanese, L. Raiteri, M. Nobile and G. Bonanno (2007). "Adult astroglia is competent for Na+/Ca2+ exchanger-operated exocytotic glutamate release triggered by mild depolarization." Journal of neurochemistry **103**(3): 1196-1207.

Parnis, J., V. Montana, I. Delgado-Martinez, V. Matyash, V. Parpura, H. Kettenmann, I. Sekler and C. Nolte (2013). "Mitochondrial Exchanger NCLX Plays a Major Role in the Intracellular Ca2+ Signaling, Gliotransmission, and Proliferation of Astrocytes." Journal of Neuroscience **33**(17): 7206-7219.

Patting, M., M. Wahl, P. Kapusta and R. Erdmann (2007). Dead-time effects in TCSPC data analysis. Photon Counting Applications, Quantum Optics, and Quantum Cryptography, International Society for Optics and Photonics.

Perry, V. H. and S. Gordon (1988). "Macrophages and microglia in the nervous system." Trends in neurosciences **11**(6): 273-277.

Rivera, C., J. Voipio, J. A. Payne, E. Ruusuvuori, H. Lahtinen, K. Lamsa, U. Pirvola, M. Saarma and K. Kaila (1999). "The K+/Cl− co-transporter KCC2 renders GABA hyperpolarizing during neuronal maturation." Nature **397**(6716): 251-255.

Rochefort, N. L. and A. Konnerth (2008). "Genetically encoded Ca2+ sensors come of age." Nature Methods **5**(9): 761-762.

Roder, P. and C. Hille (2014). "ANG-2 for quantitative Na^+ determination in living cells by time-resolved fluorescence microscopy." Photochemical & photobiological sciences **13**(12): 1699-1710.

Rojas, H., C. Colina, M. Ramos, G. Benaim, E. H. Jaffe, C. Caputo and R. DiPolo (2007). "Na+ entry via glutamate transporter activates the reverse Na+/Ca2+ exchange and triggers-induced Ca2+ release in rat cerebellar Type-1 astrocytes." Journal of neurochemistry **100**(5): 1188-1202.

Rose, C. R. (2002). "Na+ signals at central synapses." Neuroscientist **8**(6): 532-539.

Rose, C. R. (2003). "High-resolution Na+ imaging in dendrites and spines." Pflugers Arch **446**(3): 317-321.

Rose, C. R. and J. Y. Chatton (2015). "Astrocyte sodium signaling and neuro-metabolic coupling in the brain." Neuroscience.

Rose, C. R. and C. Karus (2013). "Two sides of the same coin: sodium homeostasis and signaling in astrocytes under physiological and pathophysiological conditions." Glia **61**(8): 1191-1205.

Rose, C. R. and A. Konnerth (2001). "NMDA receptor-mediated Na+ signals in spines and dendrites." Journal of Neuroscience **21**(12): 4207-4214.

Rose, C. R. and A. Konnerth (2001). "NMDA receptor-mediated Na+ signals in spines and dendrites." J Neurosci **21**(12): 4207-4214.

Rose, C. R., Y. Kovalchuk, J. Eilers and A. Konnerth (1999). "Two-photon Na+ imaging in spines and fine dendrites of central neurons." **439**(1): 201-207.

Rose, C. R. and B. R. Ransom (1996). "Intracellular sodium homeostasis in rat hippocampal astrocytes." J Physiol **491 (Pt 2)**: 291-305.

Rose, C. R. and B. R. Ransom (1997). "Gap junctions equalize intracellular Na+ concentration in astrocytes." Glia **20**(4): 299-307.

Rose, C. R., B. R. Ransom and S. G. Waxman (1997). "Pharmacological characterization of Na+ influx via voltage-gated Na+ channels in spinal cord astrocytes." J Neurophysiol **78**(6): 3249-3258.

Rose, C. R. and A. Verkhratsky (2016). "Principles of sodium homeostasis and sodium signalling in astroglia." Glia **64**(10): 1611-1627.

Rose, C. R., S. G. Waxman and B. R. Ransom (1998). "Effects of glucose deprivation, chemical hypoxia, and simulated ischemia on Na+ homeostasis in rat spinal cord astrocytes." J Neurosci **18**(10): 3554-3562.

Rutecki, P. A. (1992). "Neuronal Excitability." Journal of Clinical Neurophysiology **9**(2): 195-211.

Sagolla, K., H.-G. Löhmannsröben and C. Hille (2013). "Time-resolved fluorescence microscopy for quantitative Ca^{2+} imaging in living cells." Analytical and Bioanalytical Chemistry **405**(26): 8525-8537.

Salzer, J. L. and B. Zalc (2016). "Myelination." Current Biology **26**(20): R971-R975.

Skou, J. C. and M. Esmann (1992). "The Na,K-ATPase." Journal of Bioenergetics and Biomembranes **24**(3): 249-261.

Spruston, N. (2008). "Pyramidal neurons: dendritic structure and synaptic integration." Nat Rev Neurosci **9**(3): 206-221.

Spruston, N., Y. Schiller, G. Stuart and B. Sakmann (1995). "Activity-dependent action potential invasion and calcium influx into hippocampal CA1 dendrites." **268**(5208): 297-300.

Stokes, G. G. (1852). "XXX. On the change of refrangibility of light." Philosophical transactions of the Royal Society of London(142): 463-562.

Südhof, T. C. and J. Rizo (2011). "Synaptic vesicle exocytosis." Cold Spring Harb Perspect Biol **3**(12).

Svoboda, K., F. Helmchen, W. Denk and D. W. Tank (1999). "Spread of dendritic excitation in layer 2/3 pyramidal neurons in rat barrel cortex in vivo." Nature neuroscience **2**(1): 65-73.

Theparambil, S. M., Z. Naoshin, A. Thyssen and J. W. Deitmer (2015). "Reversed electrogenic sodium bicarbonate cotransporter 1 is the major acid loader during recovery from cytosolic alkalosis in mouse cortical astrocytes." The Journal of Physiology **593**(16): 3533-3547.

Tønnesen, J., G. Katona, B. Rózsa and U. V. Nägerl (2014). "Spine neck plasticity regulates compartmentalization of synapses." Nature neuroscience **17**(5): 678-685.

Unichenko, P., O. Myakhar and S. Kirischuk (2012). "Intracellular Na+ concentration influences short-term plasticity of glutamate transporter-mediated currents in neocortical astrocytes." Glia **60**(4): 605-614.

Untiet, V., P. Kovermann, N. J. Gerkau, T. Gensch, C. R. Rose and C. Fahlke (2017). "Glutamate transporter-associated anion channels adjust intracellular chloride concentrations during glial maturation." Glia **65**(2): 388-400.

Ventura, R. and K. M. Harris (1999). "Three-dimensional relationships between hippocampal synapses and astrocytes." Journal of Neuroscience **19**(16): 6897-6906.

Verkhratsky, A. and F. Kirchhoff (2007). "NMDA receptors in glia." The Neuroscientist **13**(1): 28-37.

Verkhratsky, A. and M. Nedergaard (2018). "Physiology of Astroglia." Physiological Reviews **98**(1): 239-389.

Virchow, R. (1970). "Gesammelte Abhandlungen zur wissenschaftlichen Medizin. Frankfurt 1856." Cp.: Gerhard Hiltner. Rudolf Virchow, Stuttgart.

Wahl, M., T. Röhlicke, S. Kulisch, S. Rohilla, B. Krämer and A. C. Hocke (2020). "Photon arrival time tagging with many channels, sub-nanosecond deadtime, very high throughput, and fiber optic remote synchronization." Review of Scientific Instruments **91**(1): 013108.

Wallraff, A., R. Köhling, U. Heinemann, M. Theis, K. Willecke and C. Steinhäuser (2006). "The impact of astrocytic gap junctional coupling on potassium buffering in the hippocampus." Journal of Neuroscience **26**(20): 5438-5447.

Walz, W. and L. Hertz (1984). "Sodium transport in astrocytes." Journal of neuroscience research **11**(3): 231-239.

Wilms, C. D., H. Schmidt and J. Eilers (2006). "Quantitative two-photon Ca^{2+} imaging via fluorescence lifetime analysis." Cell Calcium **40**(1): 73-79.

Yurinskaya, V., N. Aksenov, A. Moshkov, T. Goryachaya and A. A. Vereninov (2020). "Comparison of cellular Na+ assays by flow fluorometry with ANG-2 and flame emission: Pitfalls in using ionophores for calibrating fluorescent probes." bioRxiv.

Yuste, R. (2015). "From the neuron doctrine to neural networks." Nature Reviews Neuroscience **16**(8): 487-497.

Yuste, R., A. Majewska, S. S. Cash and W. Denk (1999). "Mechanisms of calcium influx into hippocampal spines: heterogeneity among spines, coincidence detection by NMDA receptors, and optical quantal analysis." Journal of Neuroscience **19**(6): 1976-1987.

Zadeh, I. E., J. W. Los, R. Gourgues, G. Bulgarini, S. M. Dobrovolskiy, V. Zwiller and S. N. Dorenbos (2018). "A single-photon detector with high efficiency and sub-10ps time resolution." arXiv preprint arXiv:1801.06574.

Zerangue, N. and M. P. Kavanaugh (1996). "Flux coupling in a neuronal glutamate transporter." Nature **383**(6601): 634-637.

Zheng, K., L. Bard, J. P. Reynolds, C. King, T. P. Jensen, A. V. Gourine and D. A. Rusakov (2015). "Time-Resolved Imaging Reveals Heterogeneous Landscapes of Nanomolar Ca^{2+} in Neurons and Astroglia." Neuron **88**(2): 277-288.

Zheng, K., T. P. Jensen and D. A. Rusakov (2018). "Monitoring intracellular nanomolar calcium using fluorescence lifetime imaging." Nature protocols **13**(3): 581-597.

Zheng, K., J. A. Levitt, K. Suhling and D. A. Rusakov (2014). Monitoring Nanoscale Mobility of Small Molecules in Organized Brain Tissue with Time-Resolved Fluorescence Anisotropy Imaging. Nanoscale Imaging of Synapses: New Concepts and Opportunities. U. V. Nägerl and A. Triller. New York, NY, Springer New York**:** 125-143.

Ziemens, D., F. Oschmann, N. J. Gerkau and C. R. Rose (2019). "Heterogeneity of Activity-Induced Sodium Transients between Astrocytes of the Mouse Hippocampus and Neocortex: Mechanisms and Consequences." J Neurosci **39**(14): 2620-2634.

14. Eidesstattliche Erklärung:

Ich versichere an Eides Statt, dass die vorliegende Dissertation von mir selbständig und ohne unzulässige fremde Hilfe unter Beachtung der „Grundsätze zur Sicherung guter wissenschaftlicher Praxis an der Heinrich-Heine-Universität Düsseldorf“ erstellt worden ist. Textstellen oder Abbildungen, die wörtlich oder abgewandelt aus anderen Arbeiten stammen, habe ich mit einer Quellenangabe versehen.

Diese Arbeit wurde weder vollständig noch in Teilen einem anderen Prüfungsamt zur Erlangung eines akademischen Grades vorgelegt.

Erkrath, den 27.01.2021 _____

15. Danksagung:

Hiermit möchte ich mich besonders bei Frau Prof. Dr. Christine R. Rose bedanken, die mich seit meiner Bachelorarbeit begleitet hat. Ohne ihre Empfehlung meinen Bachelor in Biologie zu beginnen wäre ich nicht an die HHU gekommen und daher sicher nicht da wo ich jetzt bin. Ich bedanke mich für stets motivierende Worte und spannende Projekte in den letzten Jahren und hoffentlich auch in der Zukunft.

Ebenfalls gilt mein Dank Herrn Prof. Dr. Christoph Fahlke, dass ich zum einen bereits während meiner Masterzeit in seinem Institut FLIM kennen lernen durfte zum anderen aber auch selbstverständlich für die Übernahme des Koreferats und des Mentorings meiner Doktorarbeit.

Herrn Dr. Karl W. Kafitz, möchte ich nicht nur für seine fachliche Betreuung, die Pflege und Bereitstellung einer exzellenten Arbeitsumgebung, sondern auch die vielen technologischen Gespräche danken.

Meinen langjährigen Kollegen Dr. Niklas Gerkau und Dr. Daniel Ziemens, möchte ich für das Bereitstellen ihrer Erfahrung, den Gesprächen und Diskussionen danken.

Ein herzliches Dankeschön geht auch an die Doktoranden die während und nach meiner Doktorandenzeit im Institut ihrer Arbeit nachgehen. Vielen Dank an, Lisa Felix, Laura Petersilie, Joel Nelson, Kathi Everaerts, und Nils Pape.

Ebenfalls danken möchte ich meiner Familie und insbesondere meinen Eltern, ohne die mein Studium auf vielerlei Arten nicht möglich gewesen wäre.

Meiner Frau Katharina möchte ich besonders Danken. Ohne den Rückhalt, das Verständnis, die Anteilnahme und all den vielen anderen Dingen, wäre ich weder der, der ich jetzt bin noch da wo ich jetzt bin.